Paleoceanography and Paleoclimatology

RESEARCH ARTICLE
10.1029/2024PA004874

Special Collection:
Illuminating a Warmer World: Insights from the Paleogene

Paleobotanical Evidence for Mediterranean Climates in the Western Canadian Paleoarctic During the Late Middle Eocene

Christopher K. West[1,2], Tammo Reichgelt[3], Alberto V. Reyes[1], Serhiy D. Buryak[1,4], Kasia J. Staniszewska[1], and James F. Basinger[5]

[1]Department of Earth and Atmospheric Sciences, University of Alberta, Edmonton, AB, Canada, [2]Royal Tyrrell Museum of Palaeontology, Drumheller, AB, Canada, [3]Department of Earth Sciences, University of Connecticut, Storrs, CT, USA, [4]Department of Physical Sciences, MacEwan University, Edmonton, AB, Canada, [5]Department of Geological Sciences, University of Saskatchewan, Saskatoon, SK, Canada

Abstract Paleogene age deposits east of the Fifteenmile River, northwest of Dawson City, Yukon, Canada preserve a diverse high-latitude fossil flora. Here, we provide new data on the age of the fossil site based on laser ablation–inductively coupled plasma–mass spectrometry (LA-ICP-MS) U-Pb dating of tephra zircons, paleobotanical paleoclimate reconstructions, and growing season length estimates based on photoperiod. These new data indicate an age of the Fifteenmile River fossil locality as late middle Eocene and likely within the Middle Eocene Climatic Optimum episode. The paleoflora-based paleoclimate reconstruction indicates the region was relatively wet and warm with non-freezing winters, but also experienced seasonal dryness, with an approximate 7 months long growing season as suggested by photoperiod. We interpret this paleoclimate as summer dry and winter wet—a climate analogous to modern day warm Mediterranean climates in the Köppen-Geiger climate classification system. These findings provide a new perspective on the past climate and environment of high-latitude ecosystems during warm greenhouse intervals and contribute to our understanding of the Earth's climate history and its potential future changes.

Key Points:

- New U-Pb data show the Fifteenmile River fossil flora age is late middle Eocene, potentially within the Middle Eocene Climatic Optimum
- West central Yukon had a warm Mediterranean climate, with wet, mild winters and a distinct summer-dry season during the late middle Eocene
- Growing season length at high latitudes during greenhouse intervals would be determined by photoperiod, not temperature

Supporting Information:

Supporting Information may be found in the online version of this article.

Correspondence to:

C. K. West,
christopher.west@gov.ab.ca

Citation:

West, C. K., Reichgelt, T., Reyes, A. V., Buryak, S. D., Staniszewska, K. J., & Basinger, J. F. (2024). Paleobotanical evidence for Mediterranean climates in the western Canadian paleoarctic during the late middle Eocene. *Paleoceanography and Paleoclimatology*, *39*, e2024PA004874. https://doi.org/10.1029/2024PA004874

Received 13 FEB 2024
Accepted 7 SEP 2024

1. Introduction

The Eocene (56–33.9 Ma) represents a time of modernization of global biota, when many plant and animal groups appeared that are still present today in our modern ecosystems; however, the Eocene is perhaps best known as a time of globally warm climate and elevated atmospheric CO_2. The Eocene Epoch was characterized by an initial warming trend that was punctuated by a series of hyperthermal events attributed to the addition of large amounts of CO_2 into the atmosphere—such as the Paleocene-Eocene Thermal Maximum (PETM), an episode of rapid global warming analogous to modern anthropogenic warming—which culminated in the Cenozoic's temperature acme (Westerhold et al., 2020; Zachos et al., 2008). Toward the late middle and late Eocene, global climate began to cool, likely as a result of declining atmospheric CO_2, leading to the decline of the hothouse and the onset of the late Cenozoic icehouse (Westerhold et al., 2020; Zachos et al., 2008). This global cooling trend from ~49 to 34 Ma led to the development of Antarctic glaciers by the early Oligocene (Bohaty & Zachos, 2003; Bohaty et al., 2009; Westerhold et al., 2020). The overall cooling trend of the latter part of the Eocene was, however, interrupted by an episode of global warmth known as the Middle Eocene Climatic Optimum (MECO) at ~40 Ma (Bijl et al., 2010; Bohaty & Zachos, 2003; Bohaty et al., 2009; Boscolo Galazzo et al., 2014; Sluijs et al., 2013; Westerhold et al., 2020; Zachos et al., 2008).

The Eocene presents an opportunity to understand the interactions between climate and biota under carbon dioxide levels higher than today, providing valuable insights into the potential impact of anthropogenic global warming (Inglis et al., 2020; Lunt et al., 2021; Tierney et al., 2022). Consequently, there is a growing body of work on Eocene-aged deposits that describe the fossil biota and the ecosystems they inhabited, and reconstruct the paleoclimate (Hollis et al., 2019 and references therein; Inglis et al., 2020; Lunt et al., 2021). The majority of these studies, however, are from the early greenhouse intervals of the Eocene such as the PETM and the Early Eocene Climatic Optimum (Inglis et al., 2020; Lunt et al., 2021). Fossil sites that preserve a record of the late middle Eocene MECO event are not nearly as well represented, and as such this interval remains largely unexplored, particularly from terrestrial sites in northern North America (Methner et al., 2016; Mulch et al., 2015), and is absent entirely from the high latitudes.

Despite significant advances in climate modeling and Eocene climate research (e.g., Inglis et al., 2020; Lunt et al., 2021; Zhu et al., 2020), our understanding of the mechanisms that underpin a global greenhouse climate remains incomplete. Most climate models are unable to reproduce the temperatures indicated at high latitudes from fossil data (e.g., Inglis et al., 2020; Lunt et al., 2021). Indeed, the mild non-freezing winter temperatures, typically above 0°C, that characterized the high latitudes during greenhouse intervals remain challenging to reconstruct accurately (e.g., Burls et al., 2021; Lunt et al., 2021). However, this is critical for understanding past greenhouse climates, as the state of the polar climate system during the winter likely had an effect on air temperature at lower latitudes, much as it does at present. Subtended to this issue are challenges in interpreting how these extinct ecosystems functioned and what potential limiting factors, if any, were operating. It is often assumed, for example, that similar to the present, temperature was the primary constraint limiting biodiversity, growing season length, and primary productivity for high-latitude greenhouse environments. However, these assumptions are too simplistic and require considerations that extend beyond the direct application of modern analogs when attempting to reconstruct extinct climates and ecosystems. In order to generate a more complete and comprehensive understanding of mechanisms and feedbacks in high-latitude climate systems of greenhouse worlds and the biota these climate systems supported, it is essential to provide additional proxy paleoclimate data from high-latitude ecosystems in the Eocene.

Plant fossils are essential for deep time terrestrial paleoclimate reconstructions. Plants are sessile organisms and therefore, unlike mobile organisms, plant phenotype reflects the environment in which it lives. In particular, traits of vegetative organs (i.e., leaves) are plastic in response to environmental stimuli (Yang et al., 2015). Leaf phenotype is a response to various environmental stressors, such as high and low light stress, water stress, heat stress, herbivory and other mechanical damage, or biochemical stress caused by toxins or other environmental pollutants. Although diverse phenotypes may be successful in a certain environment, in general, plants converge on similar phenotypes in order to survive in the same environment, commonly irrespective of taxonomy (Yang et al., 2015). These convergent strategies can therefore be recognized in leaf fossils, and then correlated to their closest modern climatic analogs.

Paleogene megafloras from Yukon, while known, have not been extensively studied (e.g., Bell, 1949; Vavrek et al., 2012; Young, 1975), and typically their age has been poorly resolved, attributed variously to the Paleocene and as young as the Oligocene. In the absence of data based on megafloral plant remains from this region, paleoclimatic and paleoenvironmental data for the early Paleogene of Yukon have come from microfloral analyses, and these are primarily qualitative (e.g., Hopkins et al., 1975; Ridgway et al., 1995), although some late Eocene Yukon palynofloras were included in a large-scale quantitative analysis by Pound and Salzmann (2017). The quantitative palynological analysis reported by Pound and Salzmann (2017) proved contradictory, as minimum temperature exceeded the maximum temperature in their reconstruction. Thus, there is a need to explore and reinvestigate Paleogene fossil megaflora sites from Yukon to provide additional data, both climatic and floristic.

One such site is the Fifteenmile River fossil locality, which is known to yield well-preserved compression/impression plant fossils (i.e., Hughes & Long, 1980; Skwara & Kurtz, 1988), but has so far remained unstudied and undescribed. As for other, similar deposits found in Yukon, the age of this deposit has been attributed to the late Paleocene (Skwara & Kurtz, 1988) to as late as the early Oligocene (Hughes & Long, 1980 and references therein). Given the paucity of high-latitude megaflora sites, resolution of the age and a reinvestigation of the Fifteenmile River fossil locality offers an opportunity to contribute significantly to our understanding of higher latitude regions during the Paleogene.

Here, we provide a multidisciplinary investigation of the Paleogene Fifteenmile River site in west-central Yukon, Canada. This includes a new age model based on LA-ICP-MS U-Pb zircon dating, and a quantitative paleoclimatic reconstruction derived from fossil plants collected from the site, offering new insights into the greenhouse climate of the western Canadian paleoarctic. Furthermore, we discuss the controls on growing season lengths in high-latitude greenhouse climates, providing photoperiod-based growing season length estimates. Lastly, we discuss the physiography of west-central Yukon during the middle Paleogene, assessing its influence on the regional climate as indicated by the fossil flora. These data enhance our understanding of the regional paleoclimate, paleoenvironment, and physiography of the western Canadian Arctic during the middle Paleogene.

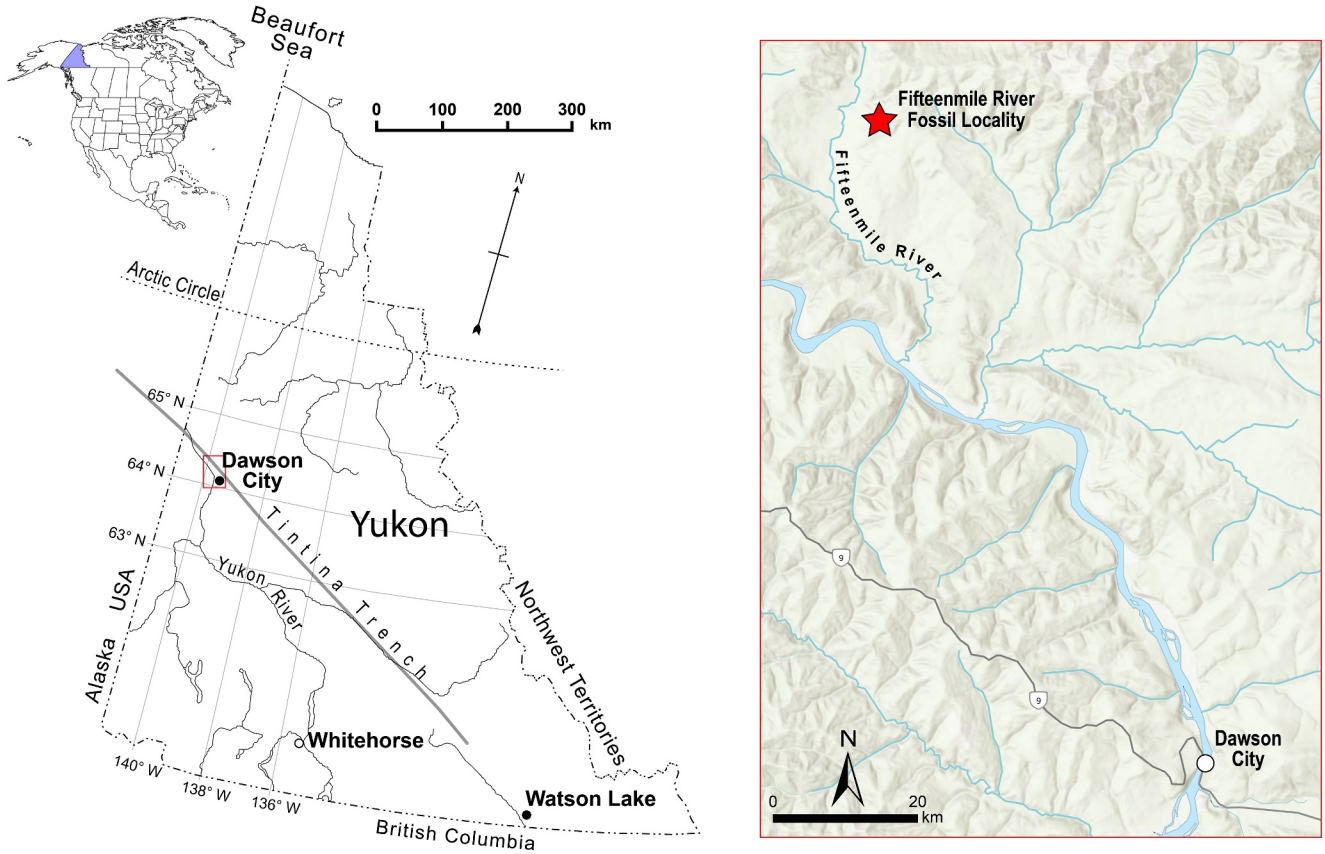

Figure 1. Map of Yukon showing the position of the Tintina Trench, Dawson City, and the Fifteenmile River fossil locality.

2. Materials and Methods

2.1. Study Area and Geological Background

The fossil plants for this study were collected from a deposit about 44 km northwest of Dawson City, Yukon, east of the Fifteenmile River, known as the Fifteenmile River fossil locality (64.41°N, 139.84°W, Figure 1). The strata are part of a series of deposits within the Tintina Trench, a major strike-slip fault extending northwest-southeast through Yukon that was affected by late Cenozoic extensional faulting (Duk-Rodkin et al., 2004; Hughes & Long, 1980). The fossil-bearing strata have been interpreted as alluvial deposits within an intermontane basin that existed during the Paleogene, and are typically best exposed along the walls of the Tintina Trench (Duk-Rodkin et al., 2004; Hughes & Long, 1980).

Hughes and Long (1980) described ~200 m of tilted strata east of the Fifteenmile River, exposed in a slump scar (Figure 2) and unconformably overlain by Plio-Pleistocene gravels and till (Duk-Rodkin et al., 2004). The strata are not currently assigned to a geological formation or group. The section was described as primarily composed of conglomerate and sandstone beds with interbedded recessive intervals of claystones, siltstones, and thin coal seams (Figure 2; Hughes & Long, 1980). The claystone beds are the primary source of compression fossil plants, but the siltstones also yield fossil plant material. The age of the fossil-bearing deposits within the Dawson City sector of the Tintina Trench has been typically regarded as late Paleocene to late Eocene based on analyses of both the micro- and megafloras (Hughes & Long, 1980; Skwara & Kurtz, 1988). In addition to the fossil plants recovered, the Fifteenmile River site also yielded the partial remains of a fossil bird discovered by J.F. Basinger (Skwara & Kurtz, 1988), with probable affinity to the Phaethontiformes (Sullivan et al., 2022), and at least one heavily devitrified tephra (Figure 2).

The modern latitude of the Fifteenmile River site is ~64°N and is considered sub-Arctic. The modern-day climate of Yukon in low-lying inland areas can be a mixture of cold climates without a dry season, with a summer-dry

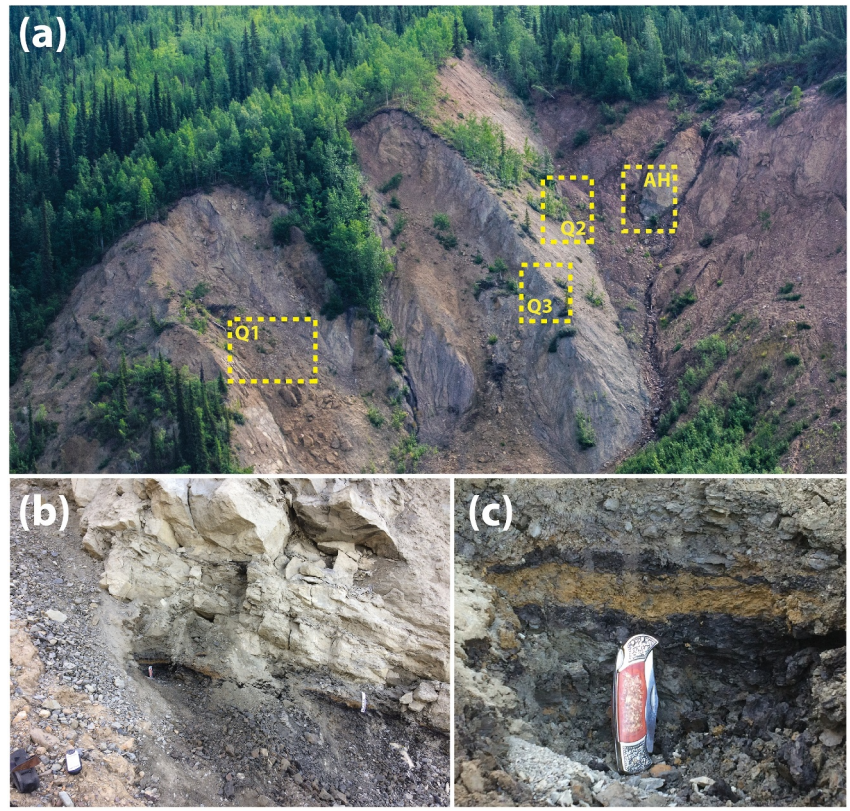

Figure 2. Overview of the Fifteenmile River fossil locality, (a) aerial view of the Fifteenmile River site and locations of quarry one (Q1), quarry two (Q2), quarry three (Q3), and the ash horizon, (b) photo of the in situ ash bed, marked by knives at the contact between intact strata and rubble, (c) close up of the ash bed.

season, or a semi-arid steppe climate (Beck et al., 2018; Taylor, 1997). The paleolatitude for the Fifteenmile River fossil locality was reconstructed using a paleolatitude calculator to be 67–68°N at ~40 Ma (van Hinsbergen et al., 2015), which indicates that the Fifteenmile River fossil locality was at or above the Arctic Circle (~66.5°N) during the middle Paleogene.

2.2. Fossil Material and Collection

Initial work for this study was based on a compression flora from Fifteenmile River in the University of Saskatchewan Palaeobotany Collection (USPC) collected in 1983. Additional fossil plant materials were collected in 2021. The recent collection represents two stratigraphically distinct localities within the local stratigraphy at Fifteenmile River. Fossil megaflora were either sampled from scree slopes that could be clearly associated with in situ strata (Q1 & Q2) or were quarried directly from in situ fossil-bearing silt and mudstone beds (Q3) (Figure 2). Material from Q2 comprises blocks reworked down the dip slope from Q3, so Q2 and Q3 are considered equivalent. Mean strike and dip measurements of the exposed alluvial strata were 106° ± 2° and 38° ± 4°, respectively. Based on these consistent structural observations and measured elevations using a laser rangefinder, Q2/Q3 is ~35 m stratigraphically above Q1. In turn, the tuff bed that provides radiometric geochronology for the Fifteenmile sequence is ~28 m stratigraphically above Q2/Q3 (Figure 2).

The original USPC fossil plant collection from 1983 was purpose-collected for determining taxonomic richness, whereas the new collections were census-collected for both paleoclimatic and paleoecological reconstructions. The USPC Fifteenmile River collection was organized into informal morphotypes to facilitate census collecting during 2021 fieldwork. In combination with this method, morphotypes were referred to established plant fossil taxa where possible, facilitating nearest living relative (NLR) taxon-based paleoclimate analysis. The fossil material collected during the 2021 field season was studied at the University of Alberta, Department of Earth and Atmospheric Sciences.

The collection was initially organized using the informal morphotypes from the USPC Fifteenmile River collection. Following this, the informal morphotype organization was further refined into the present morphotype framework (see Supporting Information S1). As part of the morphotyping process, the fossils were assigned a three-letter prefix (FMR) based on the fossil locality name and a number. Characters used to identify morphotypes followed leaf characters outlined in Ellis et al. (2009). Field and lab photography was performed using a Nikon D5300 DSLR digital camera. Fossil specimens collected at Fifteenmile River in 2021 were labeled with Yukon Palaeontology Program specimen numbers (e.g., YG ###) and will be deposited to the Yukon Palaeontology Program collection (Whitehorse, Yukon) following the completion of research.

2.3. Paleobotanical Climate Analyses

The distribution and morphology of plants is strongly influenced by climatic variables such as temperature and precipitation. Consequently, the evolutionary and ecological relationships between plants and climate can be extended into the fossil record and used to reconstruct past climates and ecosystems. The two principal methods for retrodicting past climates from fossil plants are leaf physiognomy and NLR analysis (Peppe et al., 2018).

Physiognomic methods are based on the correlation between leaf architecture (e.g., leaf size and shape, toothed or untoothed margins) and climate data derived from modern vegetation data sets. These methods include the Climate Leaf Analysis Multivariate Program (CLAMP), Leaf Area Analysis (LAA), and Leaf Margin Analysis (LMA) (e.g., Spicer et al., 2021; Wilf, 1997; Wilf et al., 1998). These methods do not require species identification, and they typically rely on a system of morphotypes (Johnson, 2002). NLR methods, such as Bioclimatic Analysis (BA) (Greenwood et al., 2005), are used to generate paleoclimatic information from fossil assemblages using the climatic range of modern-day taxa that are most closely related to the fossil taxa.

In keeping with best practice methods of paleoclimate reconstruction using fossil plants (see Hollis et al., 2019; West et al., 2020), we also use the ensemble approach to derive a consensus paleoclimate reconstruction that does not prioritize one method over another. These methods are briefly outlined below.

2.3.1. CLAMP

CLAMP is a multivariate statistical method that uses modern eudicot leaves with recorded physiognomic data (e.g., size, shape, margin states, apex and base shape) under known climate conditions. Fossil leaf assemblages are similarly scored and the paleoclimate is then reconstructed by finding the closest analog in multi-dimensional space using canonical correspondence analysis (Spicer, 2008; Spicer et al., 2021; Wolfe, 1993; Yang et al., 2011). Using the Physg3brcAZ_GRIDMet3brAZ calibration data set, we provide estimates of mean annual temperature (MAT), warm month mean temperature (WMMT), cold month mean temperature (CMMT), length of growing season, growing season precipitation (GSP), three wettest months (3WET), three driest months (3DRY), mean monthly growing season precipitation (MMGSP), and relative humidity (RH) for the Fifteenmile River fossil site (Spicer, 2008; Spicer et al., 2021; Wolfe, 1993; Yang et al., 2011).

Additionally, we obtained mean annual precipitation (MAP), warmest (WQM) and coldest (CQM) quarter mean temperatures, and driest month precipitation (DMP) from WORLDCLIM (Fick & Hijmans, 2017) for the CLAMP modern calibration data set (Yang et al., 2015) and used the standard CLAMP method (Spicer, 2008; Spicer et al., 2021; Wolfe, 1993; Yang et al., 2011) to reconstruct these variables for the Fifteenmile River fossil assemblages. CLAMP is typically calibrated using gridded climate data described in New et al. (2002), and the classic CLAMP output does not include MAP, WQM, CQM or DMP (Spicer et al., 2009). Since our aim is to compare results of independent botanical paleoclimate proxies and to generate an ensemble result (e.g., Lowe et al., 2018; West et al., 2021), the reconstructed climate variables need to be the same.

Furthermore, using a single source for gridded climate information reduces uncertainty that arises from disagreement among global climate models. CLAMP regression models used for this study are available online (West et al., 2024). We identified 40 eudicot leaf morphotypes in the Fifteenmile River flora, 39 of which were used for CLAMP and LMA, and 37 were used for LAA, which exceeds the 20 morphotype threshold required to reduce uncertainty below calibration error (Spicer, 2008; Wolfe, 1993; Yang et al., 2011).

2.3.2. Leaf Margin Analysis

LMA is based on the linear relationship between MAT and the proportion of untoothed leaves (leaf margin proportion, or LMP) in a vegetation assemblage, where a higher LMP correlates with warmer temperatures (Wilf, 1997). Equations 1–3 represent the classic LMA regression equation, a wet-site bias regression equation, and a global regression equation, respectively (Kowalski & Dilcher, 2003; Peppe et al., 2011; Wing & Greenwood, 1993). Standard error for LMA derived using Equations 1 and 2 is calculated from the number of morphotypes recognized in the fossil flora (Equation 4; see Wilf, 1997), where r is the number of morphotypes. Standard error for LMA Equation 3 is set to a minimum error of 4.8°C following Peppe et al. (2011).

$$\mathrm{MAT} = 1.141 + (30.6 \times \mathrm{LMP}) \quad (1)$$

$$\mathrm{MAT} = 2.223 + (36.3 \times \mathrm{LMP}) \quad (2)$$

$$\mathrm{MAT} = 4.6 + (20.4 \times \mathrm{LMP}) \quad (3)$$

$$\sigma MAT = 30.6\left(\sqrt{1} - \mathrm{LMP}\right)/r \quad (4)$$

2.3.3. Leaf Area Analysis

LAA uses the natural log of mean leaf area (MlnA) for a vegetation assemblage to estimate MAP (Wilf et al., 1998). For this study, leaves were measured using both a direct and indirect method. Leaf areas were calculated directly from photographs using the program ImageJ (Schneider et al., 2012) and indirectly from analog measurements using Equation 5 (Cain et al., 1956). Leaf areas calculated using the indirect method are then used in association with the Raunkiaer-Webb size class templates provided by the Manual of Leaf Architecture (Ellis et al., 2009). MAP was estimated from two linear regression equations published in Wilf et al. (1998) (Equation 6) and Peppe et al. (2011) (Equation 7). Standard error is calculated following standard practice for linear regression; however, each equation is converted from natural log values (ln) and is asymmetric as a result (Peppe et al., 2011; Wilf et al., 1998).

$$\text{Leaf Area} = 2/3 \times \mathrm{L} \times \mathrm{W} \quad (5)$$

$$\ln(\mathrm{MAP}) = 0.768 + (0.548 \times \mathrm{MlnA}) \quad (6)$$

$$\ln(\mathrm{MAP}) = 2.92 + (0.283 \times \mathrm{MlnA}) \quad (7)$$

2.3.4. Bioclimatic Analysis

BA (Greenwood et al., 2005) was used to generate paleoclimatic information from fossil assemblages using the modern-day distribution of NLRs of the taxa found in the fossil flora. Here, BA was performed by calculating probability density functions (e.g., West et al., 2020; Willard et al., 2019). Using data available online from the Global Biodiversity Information Facility (https://www.gbif.org/) we obtained geodetic coordinates for each NLR associated with the fossil megaflora from the Fifteenmile River fossil locality (Table 1). Exotic occurrences of taxa (i.e., plants found outside their native range) were filtered from the coordinate data sets. The data sets were randomly resampled to avoid regional overrepresentation in areas where many plant collections have been made (see West et al., 2020). Climatic envelopes of MAT, WQM, CQM, DMP, and MAP were then generated for each plant group by cross-referencing the remaining geodetic coordinates with gridded climate maps using the dismo package in R (Hijmans et al., 2005). A random set of over 500,000 unique extant combinations of MAT, WQM, CQM, DMP, and MAP was then generated. We then calculated the product of probabilities (f) of being represented by the taxa (t) in the Fifteenmile River fossil flora, using the means (μ) and standard deviations (σ) of their modern-day range, for each climatic variable (c) (Equation 8).

$$f(t_n) = \Pi_{i=1}^{5} \frac{1}{\sqrt{2\sigma_c^2 \times \pi}} e^{\frac{x_c - \mu_c}{2\sigma_c^2}} \quad (8)$$

Table 1
Morphotypes, Taxonomic Affinity, Plant Organ, and the Associated NLRs Used for Bioclimatic Analysis of the Fifteenmile River Megaflora

Morphotype identifier	Taxon affinity	Organ	NLR
FMR-041	*Acer* sp.	Seed	*Acer*
FMR-004	*Aesculus* sp.	Leaf	*Aesculus*
FMR-032	*Alnus* sp.	Leaf	*Alnus*
FMR-001	*Corylites/Betulites*	Leaf	Betulaceae
FMR-030	*Celtis aspera*	Leaf	*Celtis*
FMR-002 & FMR-025	*Trochodendroides* spp.	Leaf	Cercidiphyllaceae
FMR-012	*Cornus hyperborea*	Leaf	*Cornus*
FMR-053	*Coniopteris blomstrandii*	Frond	Dicksoniaceae
FMR-052	*Equisetum* sp.	Axis, leaves, tubers	*Equisetum*
FMR-051	*Glyptostrobus* sp.	Shoot	*Glyptostrobus*
FMR-029	Malvoid	Leaf	Malvaceae
FMR-050	*Metasequoia* sp.	Shoot, cone	*Metasequoia*
FMR-031	*Browniea* sp.	Leaf	Nyssaceae
FMR-015	Platanoid	Leaf	Platanaceae
FMR-047	*Craigia* sp.	Seed	Tilioideae
FMR-002 & FMR-021	*Trochodendron* spp.	Leaf	*Trochodendron*
FMR-052	*Typha* sp.	Leaf	*Typha*
FMR-005	*Ulmus* sp.	Leaf	*Ulmus*
FMR-014	*Vitiphyllum* sp.	Leaf	Vitaceae

In which x_c is some value of MAT, WQM, CQM, DMP, or MAP that generates a unique combination for which the likelihood of the taxa occurring in that climate can be calculated. The likelihood for the total number of taxa (n) combined was then calculated using Equation 9.

$$f(z) = \Pi_{i=1}^{n} t_n \tag{9}$$

The combination of MAT, WQM, CQM, DMP, and MAP with the highest $f(z)$ is considered the value most representative of the assemblage, whereas the 95% confidence interval is the maximum range of these climatic variables, with $f(z)$ ≥5% the maximum $f(z)$.

2.3.5. Ensemble Method

Although both physiognomic and NLR methods have constrained uncertainty, the results from these methods are not always consistent. Furthermore, the accuracy and validity of these methods are often compared, with some arguments suggesting preference for one method over another based on the perceived flaws or weaknesses inherent in the methods. Therefore, we use the ensemble method, which builds a consensus reconstruction based on all methods used (Lowe et al., 2018; Reichgelt et al., 2022; West et al., 2020, 2021), and avoids preferentially weighting one method over another. This methodology is the recommended best practice for paleobotanical-based climate reconstruction methods (Hollis et al., 2019; West et al., 2020).

The ensemble method not only highlights potential disparity between different proxy reconstructions but also reduces the inherent uncertainty in paleoclimate proxy usage, by generating probability density intervals that holistically and objectively represent the range of uncertainty proxy estimates (West et al., 2020). Additionally, the ensemble method produces the most consistent reconstruction from independent methods by propagating the error from each, further enhancing the reliability of the reconstructions (Reichgelt et al., 2022; West et al., 2020). Here, we use the ensemble approach to create the most parsimonious climate reconstructions from both the physiognomic and NLR results. Ensemble estimates of MAT, MAP, WQM, CQM, and DMP were produced by

bootstrapping climate data from all methods. The mean and standard deviations were resampled using $n = 1{,}000$ Monte Carlo simulations for each proxy reconstruction at each site, and the resamples were then used to create ensemble means and standard deviations. The LMA and LAA results from multiple calibrations were bootstrapped to create a single LMA and LAA result. This was done to avoid unequal weighting of LMA and LAA results in the MAT and MAP ensemble reconstructions, respectively.

2.4. Closest Climatic Analog

Closest climatic analogs, a practice employed by paleobotanists in an effort to accurately describe ancient climate, typically rely on evoking a modern region with similar temperature and precipitation as a potential modern analog. Although useful, this method has limitations in that the climatic analogs selected may not be fully representative or may be potentially misleading. We prefer to use a quantitative closest climatic analog method (West et al., 2021) that provides the closest modern climate available to the paleoclimate reconstruction for Fifteenmile River.

We generated 20,000 random geodetic coordinates (between 70°N and 70°S) and derived MAT, WQM, CQM, MAP, WMP, and DMP from Fick and Hijmans (2017) to determine which modern-day locations and their accompanying climatic zones are most similar to the late middle Eocene Fifteenmile River region. From the equation below (Equation 10), we then calculated Z-scores for MAT, MAP, temperature seasonality, and precipitation seasonality, where temperature seasonality is the difference from WQM−CQM and precipitation seasonality is the quotient of WMP/DMP. We then squared the Z-score distance between each site (X) and the Fifteenmile River (FMR) reconstruction to arrive at a total Z-score (Z_X) distance that indicates how climatically dissimilar a given climate is to the late middle Eocene Fifteenmile River.

$$Z_X = \log \sum_{n=1}^{4} \left(\left(X_c - \mu_c / \sigma_c \right) - \left(\mathrm{FMR}_c - \mu_c / \sigma_c \right) \right)^2 \tag{10}$$

In which μ_c and σ_c represent the mean and standard deviation, respectively, for each climatic variable; X_c is the climate at the site for which Z is calculated; and FMR_c is the reconstructed climate of the Fifteenmile River region. Using the Z-scores for each site an interpolated map was built using inverse distance weighting (IDW) in ArcGIS (ESRI, 2020). IDW interpolates point-specific log-transformed Z_X values, which allows us to generate heat maps that can visualize the geographic regions with modern climates that are most similar to the paleoclimate estimated from the ensemble method. The interpolated map had a cell size of 0.5° × 0.5° lat/long. The number of nearest points to determine cell value in IDW was set at 12, with a maximum distance of 1°.

2.5. Zircon U-Pb Methods

Zircon crystals from one heavily devitrified tephra stratigraphically associated (Figure 2) with the Fifteenmile River fossil sample sites (field sample number: AVR21-15M-1A) were prepared for analysis at the University of Alberta. Although heavily altered, the sample contains preserved platy glass shards (typically <10 μm in size) and abundant glass-clay aggregates in conjunction with trace amounts of euhedral zircon, apatite, magnetite, and ilmenite. The sample was sieved to isolate the <250 μm size fraction, and zircon crystals were separated using Wilfley table and heavy-liquid density separation methods (e.g., Strong & Driscoll, 2016). Zircon grains generally <40 μm in size were hand-picked from the heavy concentrate under a binocular microscope and mounted in epoxy.

The zircon U-Pb analyses were performed at University of Alberta in the Arctic Resources Geochemistry Laboratory using a RESOlution ArF 193 nm laser ablation system coupled to a Thermo Scientific Element XR magnetic sector-field (SF)-ICP-MS. Zircon crystals were ablated using a 23 μm beam for 40 s with the laser configured to a repetition rate of 5 Hz and energy density of ~3 J/cm^2 (see Table S1 in Supporting Information S1). The primary reference standard 91,500 (Wiedenbeck et al., 1995) was used for U-Pb mass bias fractionation and instrument drift correction, and Plešovice (Sláma et al., 2008) and Mud Tank (Horstwood et al., 2016) zircon crystals were employed as secondary standards (see Table S1 in Supporting Information S1). The $^{206}Pb/^{238}U$ external reproducibility for these standards is ~1–2% (2rsd), with MSWD values for the entire suite of analyses within the permissible range at 95% confidence level for the single population of replicated analyses (Mahon, 1996). All zircon analyses were corrected for common-Pb following the "^{207}Pb-method"

(Williams, 1998), with initial-Pb composition estimated from the Stacey and Kramers (1975) lead evolution model. The ages are reported with 2σ uncertainties (standard error at 95% confidence level).

The deposition age was calculated using the following three methods: (a) Bayesian modeling (Keller et al., 2018); (b) a maximum likelihood algorithm (Vermeesch, 2021); and (c) the weighted mean of the youngest group of ages that have overlapping 2σ uncertainties (Sharman et al., 2018). We calculated Bayesian deposition age estimates using priors based on uniform and triangular distributions, and MELTS zircon crystallization distributions based on kinetic and thermodynamic models (Keller et al., 2018). IsoplotR v.4.2 was used to calculate the maximum likelihood algorithm and weighted mean ages (Vermeesch, 2018).

3. Results

3.1. Fossil Morphotypes

The Fifteenmile River flora consists of a diverse assemblage of plant remains. In total 53 morphotypes were identified (refer to Text S1, Figures S1 to S53, and associated captions in Supporting Information S1). Forty of these are leaf morphotypes from woody broadleaf "dicot" angiosperms (Figure 3). The remaining 13 morphotypes belong to monocots (2 morphotypes), gymnosperms (2 morphotypes), polypodiopsids (2 morphotypes), and reproductive elements (e.g., flowers, catkins, fruits, and seeds; 7 morphotypes). Morphotypes that were aligned with existing fossil taxa used for NLR analysis and their associated NLR are listed in Table 1.

3.2. Paleoclimate

The results from all proxy estimates (i.e., LAA, LMA, CLAMP, non-standard CLAMP, BA, and Ensemble) can be found in Tables 2–4. The range of the primary suite of climatic variables estimated for the Fifteenmile River region (i.e., MAT, WQM, CQM, MAP, and DMP) are reported here. In addition, we report several standard CLAMP variables here (e.g., 3WET, 3DRY, GSP, and GSL). The MAT range for Fifteenmile River was 9.2–15.5°C with an ensemble estimate of 11.2 (±2.4) °C from all proxies. WQM had an ensemble estimate of 18.5 (±2.9) °C and CQM of 4.6 (±2.3) °C. The MAP ensemble estimate range was 81–161 cm yr^{-1} with a mean of 114 cm yr^{-1}. The DMP estimate range was 2–6 cm, with the ensemble mean estimate of 3.6 cm. The 3WET, 3DRY, and MMGSP values estimated from the standard CLAMP method were 37 (±23) cm, 20 (±6) cm, and 8.4 (±3.8) cm, respectively. Growing season length was estimated to be 7 (±1.1) months, and GSP from the standard CLAMP method was estimated to be 52 (±32) cm. The RH from the standard CLAMP method was estimated to be 82%.

3.3. Closest Climatic Analog

The results of the closest climatic analog analysis (Figure 4) show that the paleoclimate reconstruction for the Fifteenmile River flora is similar to modern regions that have temperate climates, including temperate oceanic climates (Mar del Plata, Brest, Amsterdam, Esbjerg, Canberra), humid subtropical climates (Buenos Aires, Toulouse, Sydney), warm-summer Mediterranean climates (Victoria, Seattle, A Coruña, Temuco), and hot-summer Mediterranean climate (Rome). The closest climatic analog analysis also highlighted some regions that have climates that are regarded as mixed or border climate, such as Vancouver, B.C, which fluctuates between a temperate oceanic climate and a summer-dry Mediterranean climate, as well as Melbourne, which has a temperate climate bordering on hot semi-arid climate. The strongest associations of the paleoclimate reconstruction are to the oceanic and warm-summer Mediterranean climate zones (Figure 4). Several of the temperate oceanic climates have some precipitation seasonality and show a similar pattern with drier summers and wetter winters (e.g., Brest, Mar del Plata, Buenos Aires), although they do not meet the criteria to be classified as Mediterranean.

3.4. U-Pb Results

Of the 20 zircon grains separated from the ash sample and dated, the eight youngest analyses form a coherent cluster with overlapping uncertainties ranging from 40.1 to 43.4 Ma; these ages were used for the Bayesian model and weighted mean deposition age calculations. The older tail of the age spectrum displays a heterogeneous mix of ages ranging from 50.1 to 884.7 Ma, suggesting presence of xenocrysts and/or a detrital component. The Bayesian model results here are insensitive to the choice of the prior, with triangular (40.2 ± 0.9 Ma), uniform

10.1029/2024PA004874

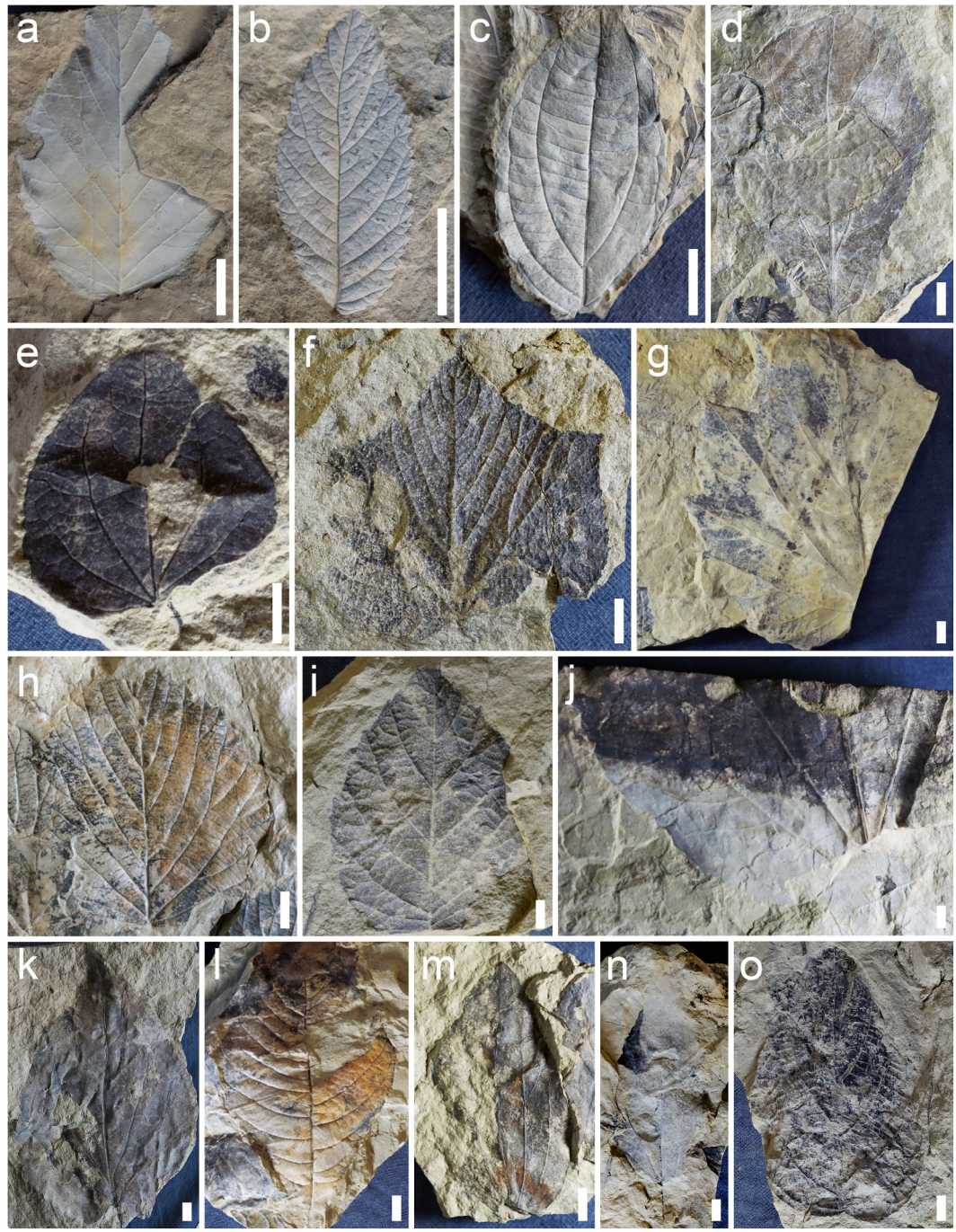

Figure 3. Examples of some of the plant fossil morphotypes found at the Fifteenmile River fossil locality. FMR = Fifteenmile River. All scales = 1 cm. (a) FMR-001 *Corylites/Betulites* YG 371.94, (b) FMR-005 *Ulmus* sp. YG 371.54a, (c) FMR-012 *Cornus hyperborea* YG 371.101b, (d) FMR-010 YG 371.166, (e) FMR-002 *Trochodendroides* sp. 1 YG 371.160b, (f) FMR-029 Malvaceae YG 372.6b, (g) FMR-027 YG 371.215a, (h) FMR-030 *Celtis* cf. *C. aspera* YG 373.27a, (i) FMR-032 *Alnus* sp. YG 372.32, (j) FMR-040 YG 371.179, (k) FMR-006, (l) FMR-004 *Aesculus* sp. YG 373.37, (m) FMR-021 *Trochodendron* sp. 2 YG 371.206b, (n) FMR-038 YG 373.7, and (o) FMR-037 YG 372.50a.

(40.1 ± 1.1 Ma) and MELTS (39.9 ± 1.4 Ma) priors yielding indistinguishable ages at 2σ uncertainty. The maximum likelihood algorithm (40.7 ± 0.5 Ma) and weighted mean (40.8 ± 0.5 Ma) results are also indistinguishable and overlap with the Bayesian model ages. For consistency we rely on the Bayesian model results, but irrespective of the method used the conclusion of the zircon geochronology remains the same. We prefer the result

Table 2
Paleoclimate Estimates of Mean Annual Temperature (MAT) and Mean Annual Precipitation (MAP) From Leaf Margin Analysis (LMA) and Leaf Area Analysis (LAA), Respectively

n	LMP	MAT (°C)	MlnA	MAP (cm yr^{-1})	Calibration
39 (37)	0.26	9.2 ± 2.2	7.64	147 (−44/+64)	Wing and Greenwood (1993) (LMA); Wilf et al. (1998) (LAA)
–	–	11.8 ± 2.6	–	–	Kowalski and Dilcher (2003)
–	–	10.0 ± 4.8	–	164 (−75/+138)	Peppe et al. (2011) (LMA and LAA)

Note. LMP = leaf margin proportion (number of taxa or morphotypes as a proportion of *n*, Wilf, 1997); MlnA = mean of the natural logarithm of leaf area. 39 of the 40 broadleaf morphotypes were useable for physiognomic analysis; an additional two morphotypes were deemed too fragmented to be accurately measured for leaf area, resulting in $n = 37$ for LAA. Standard errors for MAP are asymmetric, as they are converted from $\log_e$.

based on triangular prior (40.2 ± 0.9 Ma), because the probability density function of the $^{206}Pb/^{238}U$ ages takes roughly a triangular form and henceforth report this age is the best estimate for the tephra bed depositional age.

4. Discussion

4.1. Age of the Fifteenmile River Flora

The Paleogene deposits found within the Dawson City sector of the Tintina Trench were originally thought to be Eocene in age based on compression fossils found in the coal mines of Cliff Creek (Collier, 1903). This age assignment was later expanded by Hollick (1936), whose work on the Alaskan sector of the Tintina Trench suggested an age assignment that spanned the Late Cretaceous to Eocene. Later, Hughes and Long (1980) reported the age of the Paleogene deposits within the Dawson City sector of the Tintina Trench, including those at Fifteenmile River, as likely being late Eocene in age. This age assignment was based on previous reports by Green (1972) and Hopkins et al. (1975), who investigated the fossil-bearing horizons of coals and mudstones from nearby Cliff Creek.

Green (1972) suggested that the age of the coals and the megaflora-bearing deposits at Cliff Creek (64.54°N, 140.45°W, ∼32 km northwest of the Fifteenmile River fossil locality) were of probable Paleocene to middle Miocene age, based on the composition of the microfloras and scattered fragments of compression fossils, such as *Metasequoia occidentalis*.

Hopkins et al. (1975) further constrained the age to late Eocene, possibly earliest Oligocene, based on the microflora composition and presence of *Gothanipollis*, a pollen form genus associated with the Loranthaceae, that is primarily known from middle Eocene to Oligocene deposits in North America. Skwara and Kurtz (1988) reported that the deposits at Fifteenmile River were potentially late Paleocene in age based on an informal review of the fossil plants collected there. However, the 40.2 ± 0.9 Ma age indicated by our tephra zircon U-Pb analyses suggest a late middle Eocene age. This age is consistent with prior biostratigraphic ages for the region based on analysis of microflora from coal deposits at Cliff Creek (Hopkins et al., 1975).

The 40.2 ± 0.9 Ma tephra zircon age also falls within estimates for the age range for the MECO. The MECO is variably assigned a conservative age range of 40.1–40.5 Ma (e.g., Henehan et al., 2020; Rivero-Cuesta et al., 2019) or a broader age of 39.1–41.1 Ma (e.g., Cramwinckel et al., 2018). The more inclusive age estimate includes the full age range of increasing and decreasing temperatures into peak MECO conditions that may be spatially time transgressive, and incorporates the full age uncertainty across proxies. Disagreement between

Table 3
Paleoclimate Estimates Derived From CLAMP (n = 39)

MAT (°C) ±2.1	WMMT (°C) ±2.5	CMMT (°C) ±3.4	LGS (months) ±1.1	GSP (cm) ±32	MMGSP (cm) ±3.8	3WET (cm) ±23	3DRY (cm) ±6	RH (%) ±8.6
11.5	20.8	2.5	6.9	51.9	8.4	37.2	19.9	81.9

Note. MAT = mean annual temperature; WMMT = warm month mean temperature; CMMT = cold month mean temperature; LGS = length of growing season; GSP = growing season precipitation; MMGSP = Mean Monthly Growing Season Precipitation; 3WET = three wettest months precipitation; 3DRY = three driest months precipitation; RH = relative humidity (Spicer et al., 2021; Yang et al., 2011).

Table 4
Paleoclimate Estimates From Non-Standard CLAMP, Bioclimatic Analysis, and Ensemble Analysis

	MAT (°C)	WQM (°C)	CQM (°C)	MAP (cm·yr^{-1})	DMP (cm)
Non-standard CLAMP	9.9 (±1.6)	16.1 (±2)	3.6 (±2.6)	87.1 (63.6–119.3)	3.5 (1.8–6.6)
Bioclimatic Analysis	13.3 (11.5–15.5)	21.4 (19.2–22.6)	5.5 (2.9–8.2)	117.5 (100–141.3)	3.8 (2.6–5.5)
Ensemble Analysis	11.2 (±2.4)	18.5 (±2.9)	4.6 (±2.3)	114 (80.5–161.7)	3.6 (2.2–5.94)

Note. BA estimates represent the mean and the 95% Confidence Interval. Ensemble paleoclimate estimates are based on non-standard CLAMP, LMA, LAA, and BA. MAT = mean annual temperature; WQM = warmest quarter mean temperature; CQM = coldest quarter mean temperature; MAP = mean annual precipitation; DMP = driest month precipitation.

age estimates of "events" in Earth's history of several hundreds of thousands or even millions of years is common. An inclusive age range can incorporate the uncertainty inherent in age estimates, as well as potential spatial differences in the expression of a climate disruption. On the other hand, the more conservative age estimate may represent peak MECO conditions that are more or less consistent spatially.

The tephra used for U-Pb analyses is ~63 and ~28 m stratigraphically above the Q1 and Q2/Q3 fossil-bearing strata, respectively. Given the conformable nature of the alluvial sediments that separate the dated tuff from

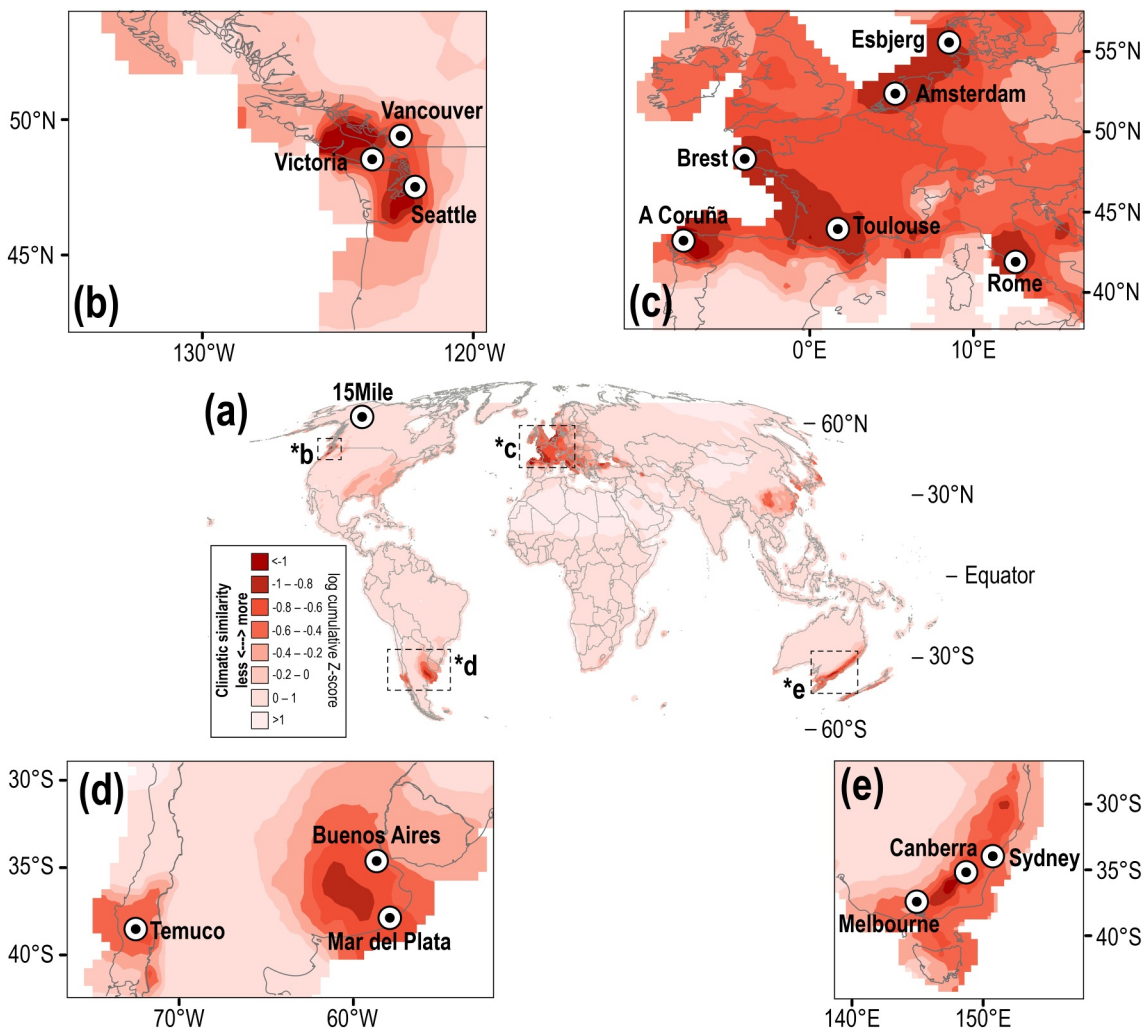

Figure 4. Climatic similarity of modern climates in the world, based on temperature and precipitation variables, to the paleoclimate of the Fifteenmile River fossil locality ca. 40 million years ago. Dashed boxes on map (a) indicate areas with the most pronounced similarity. (b) Detail of the coastal areas of the Pacific Northwest in North America, (c) western Europe, (d) southern South America, and (e) southeastern Australia.

the fossil-bearing strata, and assuming a typical alluvial sedimentation rate of 0.2–10 mm/yr (Ferring, 1986), the 63 m stratigraphic separation between the devitrified tephra and lower fossil-bearing strata represent 6.3–315 kyr. We therefore identify three sources of uncertainty in placing the Fifteenmile flora within the age constraints of the MECO: (a) the uncertain age constraints of MECO globally; (b) the ±0.9 Ma uncertainty associated with the $^{206}Pb/^{238}U$ result; and (c) the range of possible alluvial sedimentation rates that would determine the time separation of the tuff and the fossil-bearing strata. To account for these sources of uncertainty, we bootstrapped the possible ages of the Fifteenmile River flora based on the $^{206}Pb/^{238}U$ result and sedimentation rates, and evaluated the percentage of results that fall within the conservative age range of 40.1–40.5 Ma or the inclusive age range of 39.1–41.1 Ma. We generated 10,000 resamples representing possible ages of the Fifteenmile River flora assuming a normal distribution for the 40.2 ± 0.9 Ma $^{206}Pb/^{238}U$ result and random ages between 6.3 and 315 kyr representing the sedimentation rate. This resulted in 21.6% overlap of possible ages with the conservative age estimate and 71.8% overlap with the inclusive age estimate. Using a basic probability scale, it is possible that the Fifteenmile River flora was formed during the conservative age estimate (40.1–40.5 Ma) for the MECO, but likely that it was formed during the time of the more inclusive age range (39.1–41.1 Ma) for the MECO. This probabilistic approach allows us to explore different scenarios, indicating that the flora likely represents vegetation that thrived under climate conditions during, or immediately preceding or post-peak MECO, and thus different from the baseline climate that characterized the cooling trend of the late middle and late Eocene.

4.2. Paleoclimate of Fifteenmile River

The ensemble climate analysis indicates that Fifteenmile River had a temperate mesic climate (MAT = 11.2 ± 2.4°C and MAP = 114 −33.5/+47.7 cm yr^{-1}), with mild winters (CQM = 4.6 ± 2.3°C). Modern climate data for the region differ markedly from those of the late middle Eocene, particularly in the nature of cold month mean temperatures. For example, nearby Dawson City has a MAT of −4.3°C, a CMMT of −13.5°C, and a MAP of 32.4 cm yr^{-1} (Environment and Climate Change Canada, 2024), and is representative of a modern Northern Hemisphere climate, influenced by Arctic air and polar ice caps (Gervais et al., 2016), and greater mean annual ranges of temperature (Basinger et al., 1994). In contrast, due to absent high albedo and southward movement of polar air masses, the winter temperatures of ice-free greenhouse periods were altogether different and likely milder and less subject to strong day-to-day fluctuations.

Global climate model reconstructions for the late middle to late Eocene have suggested the southwestern Yukon region had a relatively mild climate, with surface air temperatures modeled between 10 and 15°C and MAP 160–200 cm (Baatsen et al., 2020). Modeled sea surface temperatures and MAP along coastal southwestern Alaska/Yukon were between 16 and 20°C and 200–300 cm respectively, which suggests increased precipitation along the coast (Baatsen et al., 2020). The results of our study are generally consistent with the Baatsen et al. (2020) model simulations, although the Fifteenmile River plant-based reconstruction yields a somewhat cooler and drier paleoclimate.

The closest climatic analog analysis (Figure 4) identifed several regions that have similar climates to the reconstructed paleoclimate for Fifteenmile River. These include temperate oceanic climates (i.e., Mar del Plata, Brest, Amsterdam, Esbjerg, Canberra), Mediterranean climates (i.e., Victoria, Seattle, A Coruña, Temuco), humid subtropical climates (i.e., Buenos Aires, Toulouse, Sydney), and regions that have mixed climates between temperate oceanic and Mediterranean (i.e., Vancouver). In the Köppen-Geiger climate system, temperate oceanic climates are defined as having the coldest month averaging above 0°C, and temperatures averaging above 10°C for at least 4 months, and a temperature average below 22°C for all months of the year (Belda et al., 2014; Peel et al., 2007). Similarly, the definition for a Mediterranean climate is that the coldest month averages above 0°C, at least 4 months averaging over 10°C, and a hot- or warm-summer Mediterranean climate with at least 1 month above 22°C, or below 22°C, respectively. The ensemble CQM (4.6°C) and WQM (18.5°C) of the Fifteenmile River flora meet the temperature criteria for both a temperate oceanic climate and a warm-summer Mediterranean climate.

In terms of precipitation, the closest climatic analog analysis largely highlighted sites that are characterized by seasonal precipitation regimes, although some sites with only minor precipitation seasonality were also highlighted by the analysis. For example, some of the temperate oceanic sites identified by the closest climatic analog analysis do have some precipitation seasonality, such as summer wet and winter dry (e.g., Buenos Aires, Mar del Plata), or are seasonally dry during the spring or fall (e.g., Amsterdam, Brest, Esbjerg). This suggests that precipitation seasonality is a common trait shared between Fifteenmile River and those sites identified by the closest climatic

analog analysis. Importantly, the definition for a temperate oceanic climate is that it does not have significant variation in precipitation between seasons (Belda et al., 2014; Peel et al., 2007), as is reconstructed for Fifteenmile River (DMP = 3.6 cm). This would disqualify the reconstructed paleoclimate for Fifteenmile River as temperate oceanic.

On the other hand, warm-summer Mediterranean climates are similar to temperate oceanic climates with respect to temperature, but differ in terms of precipitation. Instead, warm-summer Mediterranean climates have driest summer month precipitation of <4 cm, and at least three times as much precipitation in the wettest winter month (Belda et al., 2014; Peel et al., 2007). Thus, the reconstructed paleoclimate of Fifteenmile River qualifies as warm-summer Mediterranean, assuming DMP was in summer. Hot-summer Mediterranean climates are defined similarly, but must have a warmest month average >22°C (Belda et al., 2014; Peel et al., 2007), which the Fifteenmile River flora was unlikely to have had, as the ensemble WQM is 18.5°C. Humid subtropical climates are defined as having a coldest month average >0°C, an average temperature of at least 1 month >22°C, at minimum 4 months averaging >10°C, and no significant difference in precipitation between seasons, and thus an absence of dry summer months (Peel et al., 2007). The reconstructed CQM and WQM of the Fifteenmile River flora are too low to meet the criteria of a humid subtropical climate.

Modern estimates of GSP are usually representative of the warm or summer season, especially in the Northern Hemisphere, as the cold or winter seasons typically result in plant dormancy or death. Consequently, it is difficult to assign a season to estimates of GSP from past greenhouse intervals, as seasonal temperature differences were reduced and primary plant growth may not have been restricted to the astronomical summer seasons (Basinger, 1991; Basinger et al., 1994; Konrad et al., 2023; West et al., 2015; Williams et al., 2009). However, it can be assumed that the Fifteenmile River GSP estimate occurred during the astronomical summer, as the Fifteenmile River region (~67°N paleolatitude) would have been at or above the Arctic Circle during the late middle Eocene. Although not as extreme as the High Arctic, the Fifteenmile River region would have experienced lengthy periods of darkness or twilight during the winter, periods of perpetual daylight during the summer, and shoulder seasons characterized by a more typical diurnal cycle and extended intervals of twilight. Considering the greenhouse climate in place during the late middle Eocene, characterized by mild winters, reduced daily temperature fluctuations, and a narrow mean annual range of temperature, it is very likely that photoperiod, rather than temperature, was the primary control on growing season length (see Section 4.3 below), as evidenced by fossil wood anatomy (Basinger, 1991).

The GSP estimate of 52 cm, and the MMGSP of 8.4 cm, suggests the growing season length was ~6 months long (where 52 cm divided by 8.4 cm equals 6.2), which is consistent with the growing season length estimated by CLAMP (~7 months), although, as noted below, length of the growing season is influenced by photoperiod at high latitudes during periods of global warmth. Following this, if we assume a warm dry summer, as is typical with a Mediterranean climate, then the 3DRY and DMP estimates of 20 and 3.6 cm, respectively, would have occurred during an approximate six-month-long growing season. Therefore, we can conclude that the mean monthly precipitation during the growing season at Fifteenmile River would have fluctuated between 3.6 and 10.6 cm. This range assumes that the 3DRY precipitation estimate includes the DMP estimate, with $52 - 20\ \text{cm} = 32\ \text{cm}$ to be distributed over the remaining 3 months of the growing season. However, if we instead assume that the 3DRY and DMP estimates do not co-occur, and occupy instead 4 months of the growing season, the mean monthly precipitation during the growing season would range between 3.6 and 14.2 cm. As the GSP estimate accounts for approximately 46% of the MAP, the remaining 54%, or 62 cm, would be distributed across the remaining 6 months of the year. The ~62 cm of precipitation outside of the growing season would also include the 37 cm 3WET estimate, which suggests that mean monthly precipitation during the winter dark months would have been between 8.3 and 12.3 cm. Given that 12.3 cm would be the wettest winter month precipitation, which is three times the precipitation of the driest month, this suggests that the Fifteenmile River region was characterized by a Mediterranean climate during the late middle Eocene. The idea of Mediterranean climates at higher latitudes is not without merit, as parts of modern-day Yukon and Alaska currently feature summer-dry climates (Scudder, 1997; Taylor, 1997), and such summer-dry continental climates (i.e., Dsa, Dsb, Dsc, and Dsd, see Beck et al., 2018; Belda et al., 2014; Peel et al., 2007) are now typically referred to as Mediterranean-influenced climates (e.g., Mediterranean-influenced subarctic climate; Andrade & Contente, 2020; Stefanidis et al., 2022; Yalcin & Arca, 2024; Zhang et al., 2022). We note that the error range for these estimates could accommodate other precipitation combinations. However, our preferred interpretation uses the highest-probability estimates and is a mathematically consistent scenario that agrees with both our climate and closest climatic analog analysis.

This indicates that the Fifteenmile River region did not experience a pronounced winter dry season, such as would be typical for a monsoonal climate regime; however, it does suggest that the region had a summer-dry precipitation regime. Based on this interpretation, we conclude that the Fifteenmile River region had a Mediterranean or Mediterranean-like climate during the late middle Eocene, especially since the radiative flux in summer would have been disproportionately high, resulting in a higher evapotranspiration potential. The definition of a Mediterranean climate is often erroneously conflated with geography or flora (Blumler, 2005); we make no inferences with respect to geography or flora and restrict ourselves to a climatic definition alone. Broad-leaved evergreen sclerophyllous vegetation is often incorrectly assumed to be a necessary qualifier for a Mediterranean climate (Blumler, 2005; Gavilán et al., 2018; Valiente-Banuet et al., 1998), which would seem incongruent with the polar-broad leaved trees of the Paleogene as most, if not all, were deciduous (e.g., West et al., 2019). However, there are examples of sclerophyllous floras in the modern day that grow in regions without a Mediterranean climate (Valiente-Banuet et al., 1998), and regions with a Mediterranean climate that instead support a deciduous flora rather than an evergreen sclerophyllous flora (Gavilán et al., 2018). Indeed, evidence from the fossil record suggests that sclerophylly may have evolved in both winter wet and summer wet climate regimes (Denk et al., 2023). Although outside the scope of this present study, systematics and ecophysiology analyses of the fossil flora from Fifteenmile River will be subjects of future studies.

Mediterranean climates are characterized by a winter precipitation maximum. Marine west coast North American climates are also characterized by a winter precipitation maximum and are a subtype of the temperate oceanic climate type. The marine west coast climate was also indicated by the closest climatic analog analysis—although not as strongly as the Mediterranean climate. In select cases, some regions that show marine west coast climates have a mixed climate, where topographical variations (e.g., mesoscale altitude and aspect) lead to a mosaic of Mediterranean and marine west coast climates (i.e., Vancouver). Therefore, it is reasonable to conclude that the Fifteenmile River region had a Mediterranean climate, or possibly a mosaic Mediterranean and temperate oceanic climate, as evidenced by the summer-dry and winter-wet precipitation regime. Seasonally dry forests during the late middle Eocene have also been recognized in the mid-latitudes of North America (Allen et al., 2020), in South America (Martinez et al., 2021), and Australia (Reichgelt et al., 2022). Likewise, the post-MECO interval in Asia has been linked to arid episodes (Bosboom et al., 2014). Although more data are required, these studies and the results of this study suggest that the increased precipitation seasonality and aridity associated with the Eocene-Oligocene transition (Butrim & Royer, 2020) may have begun as early as the late middle Eocene.

4.3. Controls on Growing Season Length at High Latitudes

The length of the growing season in present-day, higher-latitude environments is primarily determined by temperature, with photoperiod playing a secondary role as adequate temperatures for initiating plant growth are typically available only after a threshold number of daylight hours has been reached (Hänninen, 2016; Taulavuori et al., 2009). However, the growing season, as a concept, is somewhat vague, and its definition often varies depending on specific plant responses (e.g., growth in volume or biomass, phenological stages like bud break and leaf senescence, dormancy cycles) and environmental criteria (e.g., short-term weather patterns or long-term climate trends) being evaluated (Körner et al., 2023). Nevertheless, at its root, the growing season for plants can be understood as the synchronization of phenological events with the fluctuation of favorable environmental conditions, whereby this synchronization aims to maximize photosynthesis and growth (Caffarra & Donnelly, 2011; Hänninen, 1987, 2016; Heide, 1993; Körner et al., 2023).

This is most pronounced in the seasonal climates of present-day temperate and boreal latitudes. In these regions, woody perennial plants have developed physiological mechanisms to regulate their growth cycles. They achieve this by transitioning through phases of induced dormancy, effectively synchronizing their growth with the annual variations in temperature, precipitation, and photoperiod. Dormancy is a crucial adaptation employed by temperate and boreal trees to ensure survival during extended periods of freezing temperatures in the winter months. This adaptation involves a state of suspended vegetative activity until favorable growth conditions return in the spring (Caffarra & Donnelly, 2011; Hänninen, 2016). Trees from temperate and boreal latitudes usually enter dormancy and start developing dormant buds toward the end of summer, which coincides with a decreasing photoperiod (Caffarra & Donnelly, 2011; Hänninen, 2016). These changes in photoperiod present an early indication of the impending decrease in temperatures (Battey, 2000; Caffarra & Donnelly, 2011; Hänninen, 1990). This state is known as “endo-dormancy” and is characterized by a state of suspended growth, where growth will continue to be inhibited even during favorable environmental conditions, such as an increase in

temperature (Caffarra & Donnelly, 2011; Hänninen, 2016). This state of endo-dormancy is only broken upon exposure to cold or chilling temperatures, typically temperatures below 10°C, for a set number of days that is usually species-specific (Battey, 2000; Hänninen, 2016; Sarvas, 1972). After the endo-dormancy period, trees transition into a phase known as eco-dormancy. During this phase, the tree remains resilient to freezing conditions but is no longer in a state of deep dormancy; however, growth is still hindered due to unfavorable environmental conditions (Caffarra & Donnelly, 2011; Hänninen, 2016). Subsequently, exposure to consistently warm temperatures over a certain period acts as an environmental signal to conclude the eco-dormancy phase. This prompts the tree to initiate budburst and resume its growth (Arora et al., 2003; Battey, 2000; Caffarra & Donnelly, 2011; Cannell & Smith, 1983; Hänninen, 1990, 2016; Sarvas, 1972).

Although temperature is currently the primary factor necessitating dormancy, photoperiod commonly regulates the initiation and termination of dormancy in certain tree species. Specifically, for many boreal tree species, the diminishing photoperiod often signals growth cessation (Bennie et al., 2010; Hänninen, 2016) and is interpreted as an adaptive response, preparing the trees for the eventual temperature drop that typically accompanies a reduction in photoperiod (Hänninen, 2016). Moreover, photoperiod holds a significant role in terminating dormancy for numerous boreal and northern temperate tree species. For example, an extended photoperiod characterized by longer days and shorter nights can either shorten the number of chilling days needed to break endo-dormancy (Heide, 1993; Myking & Heide, 1995), or compensate entirely for insufficient chilling (Caffarra & Donnelly, 2011; Farmer, 1968; Myking & Heide, 1995; Nienstaedt, 1967).

The ability of photoperiod to override dormancy temperature controls can be understood as a 'safety mechanism'. This mechanism comes into play when there is an insufficient number of chilling days, which might happen during a warm early spring or in a generally milder climate. In such cases, if the nights become sufficiently short, endo-dormancy will eventually be broken, allowing growth to resume as usual at the beginning of the growing season (Hänninen, 2016 and references therein).

Even so, empirical evidence for the importance of photoperiod for some tree species remains equivocal, especially when some temperate trees appear to disregard photoperiod entirely, or that for some trees fluctuating temperatures can result in changes in dormancy irrespective of photoperiod length (Caffarra & Donnelly, 2011; Hänninen, 2016; Heide, 2011; Heide & Prestrud, 2005; Junttila, 1980). Nevertheless, photoperiod is capable of modulating both the cessation and initiation of growth in plants, as would be required at higher latitudes during greenhouse intervals in Earth history. During the late middle Eocene this would have been necessary for the vegetation in the Fifteenmile River region, where winter temperatures, even during the dark polar winter, would have been mild and without sustained freezing, and would not have been sufficient to induce dormancy. Consequently, temperature would not have been a limiting factor, making photoperiod the primary factor in inducing dormancy at high latitudes.

In order to derive growing season length at Fifteenmile River during the late middle Eocene, it is necessary to evaluate the photoperiod in terms of both daylight hours and available Photosynthetically Active Radiation (PAR), and then attempt to cross-validate the growing season length estimates provided from the CLAMP analysis. This can be done using estimates of average insolation at the top of the atmosphere and the number of light hours for a specific time and place using solar data derived from the ModelE2 version of the Goddard Institute for Spaces Studies (GISS) GCM developed for the Coupled Model Intercomparison Project Phase (CMIP5) as part of the Fifth Assessment Report of the IPCC (IPCC, 2013; Schmidt et al., 2014). These data are available online (https://data.giss.nasa.gov/modelE/ar5plots/srlocat.html). This model was used because it provides data on sunrise and sunset times, average sunlight at the top of the atmosphere, and accounts for the angle of incidence of sunlight, which affects light intensity at a given latitude. The angle of incidence is crucial for accurate insolation estimates at high latitudes, where the sun's rays strike the Earth more obliquely. This oblique angle reduces the solar energy per unit area, leading to lower light intensity and influencing the effectiveness of photosynthesis and overall solar energy availability. These data were generated for the year 2023 and for a latitude of 67°N and longitude of 139°W.

Solar insolation, initially measured at the top of the Earth's atmosphere, quantifies the total amount of solar energy received per unit area and is typically expressed in watts per square meter (W/m^2). However, as solar radiation passes through the atmosphere, its intensity diminishes due to scattering and absorption, resulting in an average loss of approximately 57% (Hartmann et al., 2013). Of this attenuated solar radiation, only a fraction falls within the range of PAR (wavelengths between 400 and 700 nm) which can be absorbed by chlorophyll and other pigments to

drive the photosynthetic process. Photosynthetic Photon Flux Density (PPFD) narrows this further by quantifying the amount of PAR reaching a specific area, and is measured in micromoles of photons per square meter per second (μmol/m^2/s). PPFD quantifies the instantaneous intensity of light available for photosynthesis at a particular point, and typically conversions approximate 1 W/m^2 ≈ 4.57 μmol/m^2/s (McCree, 1972; Thimijan & Heins, 1983); however, this is assuming that the energy measured in W/m^2 is PAR only. In reality, only about 45% of solar radiation is between the 400 and 700 nm range, and it is more appropriate to use a conversion factor of ∼2.02 μmol/m^2/s (Mavi & Tupper, 2004). Daily Light Integral (DLI; mol/m^2/d) is another useful metric to measure PAR and encompasses the comprehensive energy received by a plant over a day from both the varying intensity and duration of light exposure (Poorter et al., 2019). DLI provides further information about the useable energy for photosynthesis during a 24-hr period, as it is a function of the PPFD and the total light hours (Poorter et al., 2019).

It is challenging to determine the average DLI requirements for an entire forest ecosystem, as some plant species are better adapted to shade or full sun, and both greenhouse experiments and observations in the field have shown that some plants are able to tolerate a very low DLI (∼1–6 mol/m^2/d) and still photosynthesize (Caffarra & Donnelly, 2011; Welander & Ottosson, 1997; Poorter et al., 2019 and references therein); however, experiments have shown that many plants are unable to reproduce or function well at levels below 3 mol/m^2/d (Poorter et al., 2019). Therefore, a minimum DLI threshold of 3 mol/m^2/d for the start and end of the growing season seems reasonable, as this would not compromise early reproductive efforts and capture plants capable of utilizing such low light levels, and thus capture the entirety of the growing season. Using the DLI of 3 mol/m^2/d and accounting for losses resulting from atmospheric scattering and absorption, then at an approximate latitude of 67°N, a sufficient amount of PAR would not be available at the Fifteenmile River locality until approximately 1 March, when daily average sunlight approaches ∼97 W/m^2 at the top of the atmosphere. Using that same metric, the growing season would persist until approximately 11 October when the daily average insolation at the top of the atmosphere would dip back down to ∼97 W/m^2. This would result in 225 days of sufficient PAR, or approximately 7.4 months. A DLI of less than 3 mol/m^2/d would probably be below the photosynthetic threshold for most of the plants in the Fifteenmile River forest, and is therefore considered unrealistic as the onset of the growing season. A DLI of more than 3 mol/m^2/d, on the other hand, would likely overlook many plants capable of growth under low light conditions.

It is important to remember that DLI is both a measure of light intensity (PPFD) and total light hours (i.e., photoperiod), and can be potentially misleading, as identical DLI values can occur from different combinations of PPFD and photoperiod (e.g., a DLI of 3 mol/m^2/day may result from different values of PPFD and photoperiod). This is not unimportant, as the photoperiod has been shown to have effects on dormancy induction and break regardless of light intensity (Caffarra & Donnelly, 2011; Dormling et al., 1968; Ekberg et al., 1979; Häbjørg, 1972; Hänninen, 2016; Heide, 1974; Howe et al., 1995; Junttila, 1980; Junttila & Skaret, 1990; Wareing, 1956), and both day length and night length have been shown to play a role in signaling the start and end of dormancy (Hänninen, 2016 and references therein). However, the role day length and night length play in dormancy in modern forests appear to be linked to temperature (Tanino et al., 2014) and are more challenging to use as proxies for growing season length in greenhouse worlds like the late middle Eocene.

Another important point to keep in mind is that the calculations of PPFD and DLI are based on the average sunlight striking the atmosphere and the average losses that occur due to atmospheric scattering (i.e., ∼57%), and do not consider losses due to cloud cover, or sunlight passing through a canopy, and therefore the leaf area index. Nevertheless, as temperature would not have been a limiting factor during the global greenhouse world of the Eocene it is evident that light intensity and photoperiod would have been crucial for signaling dormancy, especially at high latitudes. Thus, using the value of 3 mol/m^2/d as a reasonable threshold minimum for the initiation and cessation of the growing season, we infer a growing season length for the Fifteenmile River region of approximately 7.4 months.

The distinction between estimating growing season length using temperature versus light is more evident when considering the thresholds for these estimates. For example, the CLAMP threshold for growing season is defined as months with a mean monthly temperature of 10°C or more (Wolfe, 1993). This temperature threshold was chosen as it was considered to be the temperature boundary between forest and tundra (Wolfe, 1993 and references therein). However, a more recent study examining the controls on the treeline at high elevations and high latitudes suggested the temperature boundary for the treeline is a daily mean temperature greater than 0.9°C, with a minimum mean of 6.4°C across those days (Paulsen & Körner, 2014). Using these temperature minima the

growing season length could be as long as 365 days for the late middle Eocene Fifteenmile River locality, as well as for the early Eocene plant fossil localities known from higher latitudes, given the warm mild climates with non-freezing winters these regions exhibited (e.g., West et al., 2020). This is, of course, illogical given polar extended winter darkness at these latitudes would inhibit photosynthesis. This underscores the potential problems with defining a growing season based solely on temperature during ancient greenhouse intervals, such as those found in the Eocene, and that light played a pivotal role on both growing season length and dormancy cycles.

4.4. Mediterranean Climates and Yukon Physiography During the Late Middle Eocene

The modern summer-dry climate of the Mediterranean region, typified by hot or warm, dry summers and mild, wet winters, is primarily driven by a combination of atmospheric and physiographic factors (Lionello et al., 2006; Rundel et al., 2016). Subtropical high-pressure systems, such as the Azores High, shift northward during the summer months, which creates a descending air mass that suppresses cloud formation and precipitation. Concurrently, during the summer months the polar jet stream moves northward, which redirects synoptic storm systems away from the region, further reinforcing dry conditions. Physiographic features, including the Mediterranean Sea and surrounding mountain ranges like the Atlas Mountains in Africa and the Alps in Europe, play a significant role by moderating temperatures and blocking moist air masses from regions of the Mediterranean basin. Additionally, high summer sea surface temperatures contribute to local evaporation but generally fail to produce significant rainfall due to the stable atmospheric conditions. Seasonal wind patterns, such as the Etesian winds from the Aegean Sea, also facilitate dry conditions by transporting dry air from inland areas or high-pressure regions (Lionello et al., 2006; Rundel et al., 2016).

Collectively, these features result in a distinctive summer-dry pattern named after this region: a Mediterranean climate. However, this climate type is not restricted to the geographic Mediterranean, but occurs in other regions, including parts of California, Chile, South Africa, and Australia (Beck et al., 2018), where similar combinations of atmospheric and physiographic features result in the development of a Mediterranean climate (Conradie et al., 2022; Minnich, 2006; Rundel et al., 2016).

Summer-dry continental climates in sub-Arctic regions (Beck et al., 2018; Belda et al., 2014; Peel et al., 2007), now often referred to as "Mediterranean-influenced" climates (Andrade & Contente, 2020; Stefanidis et al., 2022; Yalcin & Arca, 2024; Zhang et al., 2022), such as those found in parts of Yukon and Alaska (Beck et al., 2018; Scudder, 1997; Taylor, 1997), result from atmospheric and physiographic interactions similar to those found at lower latitudes. During the summer months, due to irradiation and the high heat capacity of the North American continental landmass, high-pressure systems develop over the interior of the continent, resulting in a descending air mass that suppresses cloud formation and precipitation. The position and strength of the polar jet stream also play a crucial role as it shifts northward during the summer, redirecting storm systems away from these regions, which results in reduced precipitation.

Conversely, winters may receive more precipitation due to the shifting jet stream (Shields et al., 2021). Additionally, the presence of large mountain ranges, such as the St. Elias and the Coast ranges, contribute to dry conditions by blocking moist maritime air from moving inland. These areas also experience increased solar radiation during the extended daylight hours of summer, which enhances evaporation and leads to drier surface conditions (Scudder, 1997; Taylor, 1997). These combined factors create a distinct summer-dry climate, despite the higher latitude, resembling the Mediterranean pattern of warm, dry summers, and mild, wet winters.

Although the Earth's climate was considerably warmer and wetter 40 million years ago than it is today, it is likely that atmospheric and physiographic features were in place in some regions of subarctic North America to support a Mediterranean climate. For example, models suggest that the polar jet stream was present during the Eocene (Baatsen et al., 2020; Shields et al., 2021). The combination of extant factors (coastal mountain ranges and summer migration of the jet stream) could have been enhanced by the elevated Eocene summer temperatures to create the Mediterranean climate in the Yukon as is indicated by our results. Proxies for weather systems, air masses, and other synoptic-scale phenomena are generally lacking, and as a consequence much of our knowledge of these events in deep time is largely derived from climate models. Thus, while it can be assumed that broadly similar atmospheric conditions were in place during the late middle Eocene to support a Mediterranean, or Mediterranean-influenced, climate at high latitudes, these ideas are not directly testable. However, there are sufficient data and proxies available to consider the physiography of Yukon, and whether or not the St. Elias and Coast range were at a suitable elevation to cause a significant orographic effect.

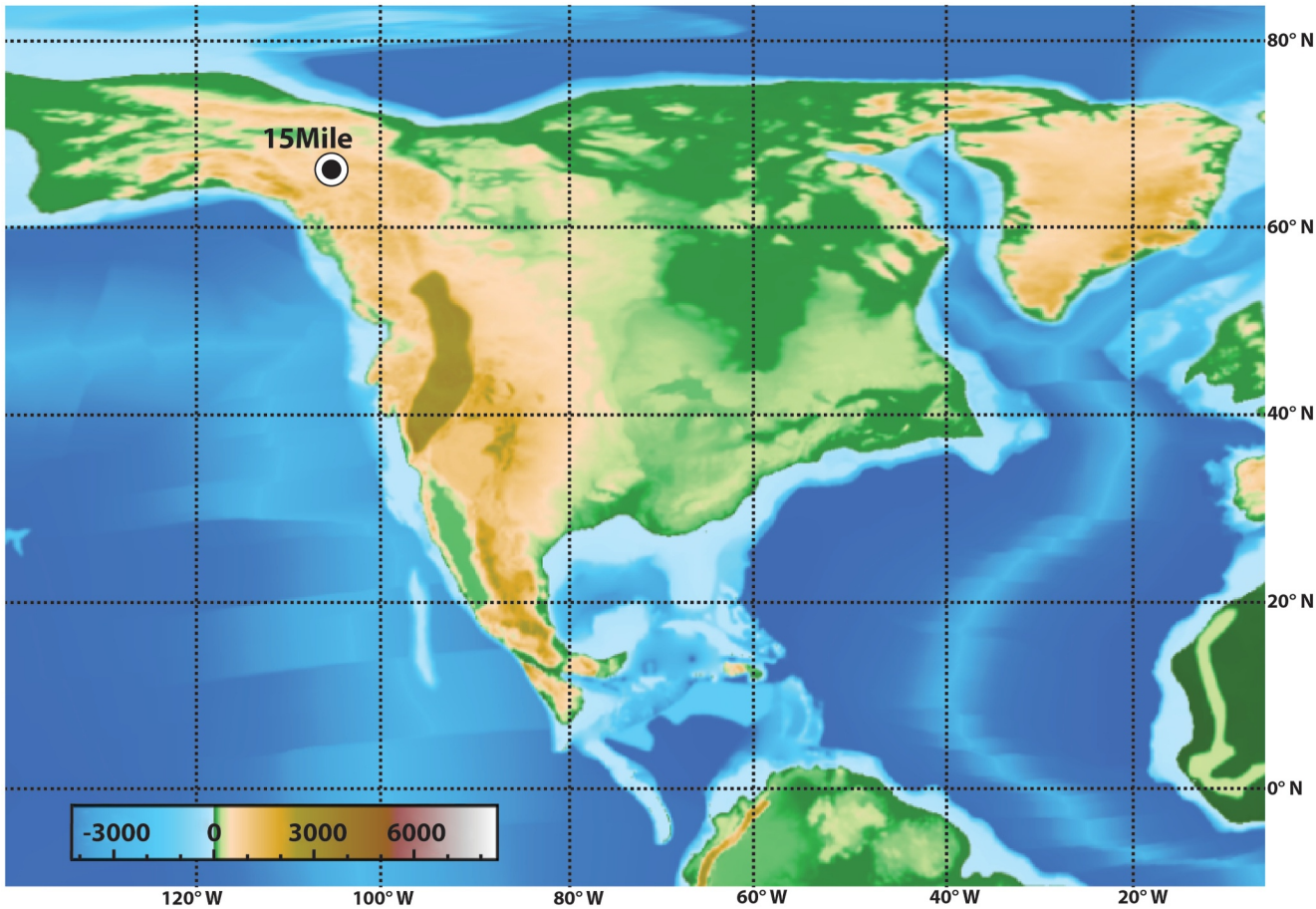

Figure 5. North American 40 Ma paleogeographic reconstruction with the approximate location of the Fifteenmile River fossil locality. Base map was generated using the online reconstruction tool (https://map.paleoenvironment.eu/) based on model reconstructions and data of Poblete et al. (2021). Gradient scale refers to the height of the topography in meters.

The current physiography of the St. Elias and Coast Range is a consequence of orogenic events that occurred between 3 and 6 Ma (e.g., Enkelmann et al., 2009; Falkowski & Enkelmann, 2016). However, uplift throughout the region likely occurred as early as the Late Cretaceous or early Paleogene (Bacon et al., 2014; Csejtey et al., 1992; Falkowski & Enkelmann, 2016; Israel & Cobbett, 2008; Mair et al., 2006; McDermott et al., 2019; Trop & Ridgway, 2007; Trop et al., 2002). These interpretations are supported by tectonic and physiographic models that suggest the regions of southeastern Alaska and southwestern and west central Yukon may have had elevations as high as 2,500 m (Figure 5) by the late middle and late Eocene (Poblete et al., 2021). Shoreline reconstructions for North America at 40 Ma (see Poblete et al., 2021) indicate that the Fifteenmile River site was about as far inland as it is currently (approx. 520 km) (Figure 5).

McDermott et al. (2019) calculated paleoelevation for the late Eocene lower Amphitheatre Formation in southwestern Yukon using the lapse rate method (see Meyer, 2007 and references therein) based on paleoclimate data sourced from palynofloral and geochemical analyses. The lapse rate method requires a temperature value for the site, where elevation is unknown, as well as a nearby contemporaneous sea surface temperature value to serve as a baseline (Meyer, 2007). McDermott et al. (2019) used a temperature of 16.7°C—the average of the maximum and minimum MAT values estimated by Pound and Salzmann (2017) for the lower Amphitheatre Formation using the Coexistence Approach—and an average sea surface temperature of 20°C, resulting in a paleoelevation estimate of ∼700 m for the Kluane Ranges in southwestern Yukon during the late Eocene. However, the incongruent minimum and maximum MAT estimates for the lower Amphitheatre Formation reported by Pound and Salzmann (2017), in addition to identified limitations in the Coexistence Approach (Grimm & Denk, 2012; Grimm & Potts, 2016; Grimm et al., 2016), suggest that this paleoelevation estimate might be problematic.

Re-evaluation of the late Eocene (~38 Ma) palynoflora of the lower Amphitheatre Formation from Ridgway et al. (1995) using BA provides a MAT estimate (~12°C, see Tables S4 and S5 in Supporting Information S1) several degrees cooler than the MAT used by Pound and Salzmann (2017) to determine paleoelevation of the Kluane Range. Using the same variables for sea surface temperature, lapse rate, and sea level used by McDermott et al. (2019), we derive a paleoelevation of about ~1,500 m for the lower Amphitheatre Formation in the Kluane Range during the late Eocene, as compared to current elevations which vary between 2000 and 2,800 m, with an approximate average elevation of 1,700 m. This calculated paleoelevation is substantially higher than the ~700 m paleoelevation estimate of McDermott et al. (2019), but lower than the 2,000–2,500 m paleoelevation reported in recent paleo-physiographic models (Poblete et al., 2021).

These paleoelevation estimates, coupled with paleogeographic models, indicate some orographic influence on precipitation along the southwest coast of Yukon. This would have reduced the amount of precipitation available to the Fifteenmile River region during the late middle Eocene. Indeed, the reconstructed paleo-elevation of ~1,500 m is consistent with the inferred uplift of the Yukon-Tanana plateau region—which includes the Fifteenmile River fossil locality—as early as the Late Cretaceous (Mair et al., 2006; Pavlis, 1989; Trop et al., 2019). This is higher than the current elevation of the Fifteenmile River site of approximately 740 m. Furthermore, a sizable Yukon-Tanana plateau during the late middle Eocene would have resulted in air mass desaturation, which would have further contributed to the generation of an inland Mediterranean, or Mediterranean-influenced, climate some distance from the paleo-coast. Finally, during globally warmer periods, the North American west coast is recognized as an area with increased winter moisture transport through atmospheric rivers (Shields et al., 2021), which suggests enhanced winter precipitation in these regions. Curiously, Mediterranean climates at elevations of 800–1,500 m, such as those found at present in California and the mountains of southeastern Australia (Beck et al., 2018; Kelly & Goulden, 2016), are some of the closest modern climate analogs to the reconstruction based on the Fifteenmile River flora (Figure 4). These results suggest that the physiographic and climatic conditions in the Eocene Yukon were conducive to the development of a Mediterranean, or Mediterranean-influenced, climate.

5. Conclusions

The present study provides new U-Pb age and paleoclimate data for a terrestrial high-latitude and high-altitude fossil site from Yukon, Canada. Zircon U-Pb analyses from a tephra interbedded in alluvial sediments at Fifteenmile River provide an age of 40.2 ± 0.9 Ma, which indicates that the fossil flora used for this study were growing during the late middle Eocene, an age that encompasses the MECO. Considering the duration of the MECO event and an average sedimentation rate, we conclude that it is likely that the fossil flora from the Fifteenmile River represents vegetation growing during, or immediately prior to or post-peak MECO. The ensemble paleoclimate estimates from both physiognomic and BA indicate a warm paleoclimate (MAT = 11.2°C) for the Fifteenmile River region, with mild winters (CQM = 4.6°C). Although relatively wet (MAP = 114 cm yr^{-1}), the region experienced precipitation seasonality (3DRY = 20 cm, 3WET = 37 cm) characterized by a distinct summer-dry season (DMP = 3.6 cm). Estimates of growing season using both light intensity and photoperiod suggest a growing season approximately 7.4 months in length. Temperature-based estimates of growing season, such as those derived from CLAMP, are not relevant to high-paleolatitude sites such as Fifteenmile River, with their mild, yet dark winters. Closest climatic analog analysis indicates that regions with a Mediterranean climate are the most similar modern analogs. A Mediterranean climate may have resulted from uplift of a proto-coastal mountain range along the coast of southwestern Yukon during the late middle Eocene, or to the Fifteenmile River region itself having been at moderate elevation as part of an upland plateau. These interpretations align with previous GCM climate and paleogeographic models (Baatsen et al., 2020; Poblete et al., 2021), and when taken together, provide a more comprehensive understanding of high-latitude environments and climate in North America during the final greenhouse event of the Eocene—an event superimposed upon the global cooling trend that would define global climate for the remainder of the Paleogene Period and the entirety of the subsequent Neogene Period.

Conflict of Interest

The authors declare no conflicts of interest relevant to this study.

Data Availability Statement

Physiognomic and associated data used for LAA, LMA, and CLAMP paleoclimate analysis are available at the Mendeley open-access data repository (West et al., 2024). Geodetic coordinate data for modern plants are available online from the Global Biodiversity Information Facility, https://www.gbif.org (retrieved 13 January 2022), specific occurrence data doi used for this study are downloadable from West et al. (2024). Model estimates of average insolation and light hours are available from the NASA Goddard Institute for Space Studies and are accessible online at https://data.giss.nasa.gov/modelE/ar5plots/srlocat.html (retrieved 15 August 2023). Physiographic data used for modeling are published in Poblete et al. (2021) and available online at https://map.paleoenvironment.eu/. Data published in Ridgway et al. (1995) were used in support of this research.

Acknowledgments
The research at Fifteenmile River was done under permits issued to CKW from the Yukon Government (21-34S&E) and Tr'ondek Hwech'in First Nation. CKW acknowledges a private donor for funding the Climates of the Canadian North Postdoctoral Fellowship while at the University of Alberta. We thank the Polar Continental Shelf Program (project 612-18), Grant Zazula and Elizabeth Hall (Yukon Palaeontology Program), and Ross MacPhee for supporting earlier reconnaissance investigations at Fifteenmile River. We thank Beverley Wallis for assistance during the 2021 field season. SDB thanks Yan Luo and Graham Pearson for facilitating zircon U-Pb dating at the Arctic Resources Geochemistry Laboratory. CKW thanks Hailey Schmitke for assistance with ArcGIS. The research was supported by NSERC Discovery and Northern Research Supplement grants to AVR and JFB. We thank the two reviewers, the associate editor, and the editor-in-chief for their detailed comments and engagement with the manuscript.

References

Allen, S. E., Lowe, A. J., Peppe, D. J., & Meyer, H. W. (2020). Paleoclimate and paleoecology of the latest Eocene Florissant flora of central Colorado, USA. *Palaeogeography, Palaeoclimatology, Palaeoecology*, *551*, 109678. https://doi.org/10.1016/j.palaeo.2020.109678

Andrade, C., & Contente, J. (2020). Köppen's climate classification projections for the Iberian Peninsula. *Climate Research*, *81*, 71–89. https://doi.org/10.3354/cr01604

Arora, R., Rowland, L. J., & Tanino, K. (2003). Induction and release of bud dormancy in woody perennials: A science comes of age. *HortScience*, *38*(5), 911–921. https://doi.org/10.21273/HORTSCI.38.5.911

Baatsen, M., Von Der Heydt, A. S., Huber, M., Kliphuis, M. A., Bijl, P. K., Sluijs, A., & Dijkstra, H. A. (2020). The middle to late Eocene greenhouse climate modelled using the CESM 1.0. 5. *Climate of the Past*, *16*(6), 2573–2597. https://doi.org/10.5194/cp-16-2573-2020

Bacon, C. R., Dusel-Bacon, C., Aleinikoff, J. N., & Slack, J. F. (2014). The Late Cretaceous Middle Fork caldera, its resurgent intrusion, and enduring landscape stability in east-central Alaska. *Geosphere*, *10*(6), 1432–1455. https://doi.org/10.1130/GES01037.1

Basinger, J. F. (1991). The fossil forests of the Buchanan Lake Formation (early Tertiary), Axel Heiberg Island, Arctic Archipelago: Preliminary floristics and paleoclimate. *Geological Survey of Canada Bulletin*, *403*, 39–66.

Basinger, J. F., Greenwood, D. R., & Sweda, T. (1994). Early Tertiary vegetation of Arctic Canada and its relevance to paleoclimatic interpretation. In *Cenozoic plants and climates of the Arctic* (pp. 175–198). Springer Berlin Heidelberg.

Battey, N. H. (2000). Aspects of seasonality. *Journal of Experimental Botany*, *51*(352), 1769–1780. https://doi.org/10.1093/jexbot/51.352.1769

Beck, H. E., Zimmermann, N. E., McVicar, T. R., Vergopolan, N., Berg, A., & Wood, E. F. (2018). Present and future Köppen-Geiger climate classification maps at 1-km resolution. *Scientific Data*, *5*(1), 1–12. https://doi.org/10.1038/sdata.2018.214

Belda, M., Holtanová, E., Halenka, T., & Kalvová, J. (2014). Climate classification revisited: From Köppen to Trewartha. *Climate Research*, *59*(1), 1–13. https://doi.org/10.3354/cr01204

Bell, W. A. (1949). *Uppermost cretaceous and Paleocene floras of western Alberta* (pp. 1–231). Geological Survey of Canada, Bulletin. (13). https://doi.org/10.4095/101514

Bennie, J., Kubin, E., Wiltshire, A., Huntley, B., & Baxter, R. (2010). Predicting spatial and temporal patterns of bud-burst and spring frost risk in north-west Europe: The implications of local adaptation to climate. *Global Change Biology*, *16*(5), 1503–1514. https://doi.org/10.1111/j.1365-2486.2009.02095.x

Bijl, P. K., Houben, A. J., Schouten, S., Bohaty, S. M., Sluijs, A., Reichart, G. J., et al. (2010). Transient middle Eocene atmospheric CO_2 and temperature variations. *Science*, *330*(6005), 819–821. https://doi.org/10.1126/science.119365

Blumler, M. A. (2005). Three conflated definitions of Mediterranean climates. *Middle States Geographer*, *38*(1), 52–60.

Bohaty, S. M., & Zachos, J. C. (2003). Significant Southern Ocean warming event in the late middle Eocene. *Geology*, *31*(11), 1017–1020. https://doi.org/10.1130/G19800.1

Bohaty, S. M., Zachos, J. C., Florindo, F., & Delaney, M. L. (2009). Coupled greenhouse warming and deep-sea acidification in the middle Eocene. *Paleoceanography*, *24*(2), PA2207. https://doi.org/10.1029/2008PA001676

Bosboom, R. E., Abels, H. A., Hoorn, C., van den Berg, B. C., Guo, Z., & Dupont-Nivet, G. (2014). Aridification in continental Asia after the middle Eocene climatic optimum (MECO). *Earth and Planetary Science Letters*, *389*, 34–42. https://doi.org/10.1016/j.epsl.2013.12.014

Boscolo Galazzo, F., Thomas, E., Pagani, M., Warren, C., Luciani, V., & Giusberti, L. (2014). The middle Eocene climatic optimum (MECO): A multiproxy record of paleoceanographic changes in the southeast Atlantic (ODP Site 1263, Walvis Ridge). *Paleoceanography*, *29*(12), 1143–1161. https://doi.org/10.1002/2014PA002670

Burls, N. J., Bradshaw, C. D., De Boer, A. M., Herold, N., Huber, M., Pound, M., et al. (2021). Simulating Miocene warmth: Insights from an opportunistic multi-model ensemble (MioMIP1). *Paleoceanography and Paleoclimatology*, *36*(5), e2020PA004054. https://doi.org/10.1029/2020PA004054

Butrim, M. J., & Royer, D. L. (2020). Leaf-economic strategies across the Eocene–Oligocene transition correlate with dry season precipitation and paleoelevation. *American Journal of Botany*, *107*(12), 1772–1785. https://doi.org/10.1002/ajb2.1580

Caffarra, A., & Donnelly, A. (2011). The ecological significance of phenology in four different tree species: Effects of light and temperature on bud burst. *International Journal of Biometeorology*, *55*(5), 711–721. https://doi.org/10.1007/s00484-010-0386-1

Cain, S. A., de Oliveira Castro, G. M., Pires, J. M., & da Silva, N. T. (1956). Application of some phytosociological techniques to Brazilian rain forest. *American Journal of Botany*, *43*(10), 911–941. https://doi.org/10.1002/j.1537-2197.1956.tb11184.x

Cannell, M. G. R., & Smith, R. I. (1983). Thermal time, chill days and prediction of budburst in Picea sitchensis. *Journal of Applied Ecology*, *20*(3), 951–963. https://doi.org/10.2307/2403139

Collier, A. J. (1903). The coal resources of the Yukon, Alaska. *U.S. Geological Survey, Bulletin 218, Series A, Economic Geology*, *26*, 1–71. https://doi.org/10.3133/b218

Conradie, W. S., Wolski, P., & Hewitson, B. C. (2022). Spatial heterogeneity in rain-bearing winds, seasonality and rainfall variability in southern Africa's winter rainfall zone. *Advances in Statistical Climatology, Meteorology and Oceanography*, *8*(1), 31–62. https://doi.org/10.5194/ascmo-8-31-2022

Cramwinckel, M. J., Huber, M., Kocken, I. J., Agnini, C., Bijl, P. K., Bohaty, S. M., et al. (2018). Synchronous tropical and polar temperature evolution in the Eocene. *Nature*, *559*(7714), 382–386. https://doi.org/10.1038/s41586-018-0272-2

Csejtey, B., Mullen, M. W., Cox, D. P., & Stricker, G. D. (1992). *Geology and geochronology of the Healy quadrangle, south-central Alaska*. U.S. Geological Survey Miscellaneous Investigation. Map I-1961, scale 1:250,000. https://doi.org/10.3133/i1961

Denk, T., Bouchal, J. M., Güner, H. T., Coiro, M., Butzmann, R., Pigg, K. B., & Tiffney, B. H. (2023). Cenozoic migration of a desert plant lineage across the North Atlantic. *New Phytologist*, *238*(6), 2668–2684. https://doi.org/10.1111/nph.18743

Dormling, I., Gustafsson, Å., & von Wettstein, D. (1968). The experimental control of the life cycle in *Picea abies* (L.) Karst. I. Some basic experiments on the vegetative cycle. *Silvae Genetica*, *17*, 44–64.

Duk-Rodkin, A., Barendregt, R. W., Froese, D. G., Weber, F., Enkin, R., Smith, I. R., et al. (2004). Timing and extent of Plio-Pleistocene glaciations in north-western Canada and east-central Alaska. *Developments in Quaternary Sciences*, *2*, 313–345. https://doi.org/10.1016/S1571-0866(04)80206-9

Ekberg, I., Eriksson, G., & Dormling, I. (1979). Photoperiodic reactions in conifer species. *Holarctic Ecology*, *2*(4), 255–263. https://doi.org/10.1111/j.1600-0587.1979.tb01297.x

Ellis, B., Daly, D. C., Hickey, L. J., Johnson, K. R., Mitchell, J. D., Wilf, P., & Wing, S. L. (2009). *Manual of leaf architecture*. Cornell University Press.

Enkelmann, E., Zeitler, P. K., Pavlis, T. L., Garver, J. I., & Ridgway, K. D. (2009). Intense localized rock uplift and erosion in the St Elias orogen of Alaska. *Nature Geoscience*, *2*(5), 360–363. https://doi.org/10.1038/ngeo502

Environment and Climate Change Canada. (2024). Canadian climate normals 1981-2010 station data, Dawson A. Retrieved from https://climate.weather.gc.ca/climate_normals/index_e.html

ESRI. (2020). ArcGIS Pro (Version 2.5). ESRI Inc. https://www.esri.com/en-us/arcgis/products/arcgis-pro/overview

Falkowski, S., & Enkelmann, E. (2016). Upper-crustal cooling of the Wrangellia composite terrane in the northern St. Elias Mountains, western Canada. *Lithosphere*, *8*(4), 359–378. https://doi.org/10.1130/L508.1

Farmer, R. E., Jr. (1968). Sweetgum dormancy release: Effects of chilling, photoperiod, and genotype. *Physiologia Plantarum*, *21*(6), 1241–1248. https://doi.org/10.1111/j.1399-3054.1968.tb07355.x

Ferring, C. R. (1986). Rates of fluvial sedimentation: Implications for archaeological variability. *Geoarchaeology*, *1*(3), 259–274. https://doi.org/10.1002/gea.3340010303

Fick, S. E., & Hijmans, R. J. (2017). WorldClim 2: New 1-km spatial resolution climate surfaces for global land areas. *International Journal of Climatology*, *37*(12), 4302–4315. https://doi.org/10.1002/joc.5086

Gavilán, R. G., Vilches, B., Gutiérrez-Girón, A., Blanquer, J. M., & Escudero, A. (2018). Sclerophyllous versus deciduous forests in the Iberian Peninsula: A standard case of Mediterranean climatic vegetation distribution. In *Geographical changes in vegetation and plant functional types* (pp. 101–116). https://doi.org/10.1007/978-3-319-68738-4_5

Gervais, M., Atallah, E., Gyakum, J. R., & Tremblay, L. B. (2016). Arctic air masses in a warming world. *Journal of Climate*, *29*(7), 2359–2373. https://doi.org/10.1175/JCLI-D-15-0499.1

Green, L. H. (1972). *Geology of Nash Creek, Larsen Creek and Dawson map-areas, Yukon Territory* (p. 364). Geological Survey of Canada. https://doi.org/10.4095/100697

Greenwood, D. R., Archibald, S. B., Mathewes, R. W., & Moss, P. T. (2005). Fossil biotas from the Okanagan Highlands, southern British Columbia and northeastern Washington State: Climates and ecosystems across an Eocene landscape. *Canadian Journal of Earth Sciences*, *42*(2), 167–185. https://doi.org/10.1139/e04-100

Grimm, G. W., Bouchal, J. M., Denk, T., & Potts, A. (2016). Fables and foibles: A critical analysis of the Palaeoflora database and the Coexistence Approach for palaeoclimate reconstruction. *Review of Palaeobotany and Palynology*, *233*, 216–235. https://doi.org/10.1016/j.revpalbo.2016.07.001

Grimm, G. W., & Denk, T. (2012). Reliability and resolution of the coexistence approach—A revalidation using modern-day data. *Review of Palaeobotany and Palynology*, *172*, 33–47. https://doi.org/10.1016/j.revpalbo.2012.01.006

Grimm, G. W., & Potts, A. J. (2016). Fallacies and fantasies: The theoretical underpinnings of the Coexistence Approach for palaeoclimate reconstruction. *Climate of the Past*, *12*(3), 611–622. https://doi.org/10.5194/cp-12-611-2016

Häbjørg, A. (1972). Effects of photoperiod and temperature on growth and development of three latitudinal and three altitudinal populations of *Betula pubescens* Ehrh. *Scientific Reports of the Agricultural University of Norway*, *51*(2), 27.

Hänninen, H. (1987). Effects of temperature on dormancy release in woody plants: Implications of prevailing models. *Silva Fennica*, *21*(3), 279–299. https://doi.org/10.14214/sf.a15476

Hänninen, H. (1990). Modelling bud dormancy release in trees from cool and temperate regions. *Acta Forestalia Fennica*, *213*, 1–47. https://doi.org/10.14214/aff.7660

Hänninen, H. (2016). Boreal and temperate trees in a changing climate. In *Biometeorology*. Springer. https://doi.org/10.1007/978-94-017-7549-6

Hartmann, D. L., Klein Tank, A. M. G., Rusticucci, M., Alexander, L. V., Brönnimann, S., Charabi, Y. A. R., et al. (2013). Chapter 2: Observations: Atmosphere and surface. *IPCC AR5 WG1*, *2013*, 159–254.

Heide, O. M. (1974). Growth and dormancy in Norway spruce ecotypes (*Picea abies*) I. Interaction of photoperiod and temperature. *Physiologia Plantarum*, *30*(1), 1–12. https://doi.org/10.1111/j.1399-3054.1974.tb04983.x

Heide, O. M. (1993). Daylength and thermal time responses of budburst during dormancy release in some northern deciduous trees. *Physiologia Plantarum*, *88*(4), 531–540. https://doi.org/10.1111/j.1399-3054.1993.tb01368.x

Heide, O. M. (2011). Temperature rather than photoperiod controls growth cessation and dormancy in *Sorbus* species. *Journal of Experimental Botany*, *26*(15), 5397–5404. https://doi.org/10.1093/jxb/err213

Heide, O. M., & Prestrud, A. K. (2005). Low temperature, but not photoperiod, controls growth cessation and dormancy induction and release in apple and pear. *Tree Physiology*, *25*(1), 109–114. https://doi.org/10.1093/treephys/25.1.109

Henehan, M. J., Edgar, K. M., Foster, G. L., Penman, D. E., Hull, P. M., Greenop, R., et al. (2020). Revisiting the Middle Eocene Climatic Optimum "Carbon Cycle Conundrum" with new estimates of atmospheric pCO_2 from boron isotopes. *Paleoceanography and Paleoclimatology*, *35*(6), e2019PA003713. https://doi.org/10.1029/2019PA003713

Hijmans, R. J., Cameron, S. E., Parra, J. L., Jones, P. G., & Jarvis, A. (2005). Very high resolution interpolated climate surfaces for global land areas. *International Journal of Climatology: A Journal of the Royal Meteorological Society*, *25*(15), 1965–1978. https://doi.org/10.1002/joc.1276

Hollick, C. A. (1936). *The Tertiary floras of Alaska*. U.S.Department of the Interior, Geological Survey. Professional Paper 182. https://doi.org/10.3133/pp182

Hollis, C. J., Dunkley Jones, T., Anagnostou, E., Bijl, P. K., Cramwinckel, M. J., Cui, Y., et al. (2019). The DeepMIP contribution to PMIP4: Methodologies for selection, compilation and analysis of latest Paleocene and early Eocene climate proxy data, incorporating version 0.1 of the DeepMIP database. *Geoscientific Model Development*, *12*(7), 3149–3206. https://doi.org/10.5194/gmd-12-3149-2019

Hopkins, W. S., Jr., Hughes, O. L., & Milner, M. (1975). *Some coal-bearing Eocene sediments and comments on their combined microflora, Cliff Creek, Yukon Territory* (pp. 37–39). Geological Survey of Canada. Paper, 75–1C. https://doi.org/10.4095/103028

Horstwood, M. S., Košler, J., Gehrels, G., Jackson, S. E., McLean, N. M., Paton, C., et al. (2016). Community-derived standards for LA-ICP-MS U-(Th-) Pb geochronology–Uncertainty propagation, age interpretation and data reporting. *Geostandards and Geoanalytical Research*, *40*(3), 311–332. https://doi.org/10.1111/j.1751-908X.2016.00379.x

Howe, G. T., Hackett, W. P., Furnier, G. R., & Klevorn, R. E. (1995). Photoperiodic responses of a northern and southern ecotype of black cottonwood. *Physiologia Plantarum*, *93*(4), 695–708. https://doi.org/10.1034/j.1399-3054.1995.930417.x

Hughes, J. D., & Long, D. G. F. (1980). *Geology and coal resource potential of early Tertiary strata along Tintina Trench, Yukon Territory*. Geological Survey of Canada. Paper 79–32. https://doi.org/10.4095/102163

Inglis, G. N., Bragg, F., Burls, N. J., Cramwinckel, M. J., Evans, D., Foster, G. L., et al. (2020). Global mean surface temperature and climate sensitivity of the early Eocene Climatic Optimum (EECO), Paleocene–Eocene Thermal Maximum (PETM), and latest Paleocene. *Climate of the Past*, *16*(5), 1953–1968. https://doi.org/10.5194/cp-16-1953-2020

IPCC. (2013). In T. F. Stocker, D. Qin, G. K. Plattner, M. Tignor, S. K. Allen, J. Boschung, et al. (Eds.), *Climate change 2013: The physical science basis. Contribution of working group I to the fifth assessment report of the intergovernmental panel on climate change*. Cambridge University Press.

Israel, S., & Cobbett, R. (2008). Kluane ranges bedrock geology, white river area (parts of NTS 115F/9, 15 and 16; 115G/12 and 115K/1, 2). In D. S. Emond, L. R. Blackburn, R. P. Hill, & L. H. Weston (Eds.), *Yukon exploration and geology 2007* (pp. 153–167). Yukon Geological Survey.

Johnson, K. R. (2002). Megaflora of the Hell Creek and lower Fort Union Formations in the western Dakotas: Vegetational response to climate change, the Cretaceous-Tertiary boundary event, and rapid marine transgression. Special Paper. *Geological Society of America*, *361*, 329–391. https://doi.org/10.1130/0-8137-2361-2.329

Junttila, O. (1980). Effect of photoperiod and temperature on apical growth cessation in two ecotypes of Salix and Betula. *Physiologia Plantarum*, *48*(3), 347–352. https://doi.org/10.1111/j.1399-3054.1980.tb03266.x

Junttila, O., & Skaret, G. (1990). Growth and survival of seedlings of various *Picea* species under northern climatic conditions. *Scandinavian Journal of Forest Science*, *5*(1–4), 69–81. https://doi.org/10.1080/02827589009382594

Keller, C. B., Schoene, B., & Samperton, K. M. (2018). A stochastic sampling approach to zircon eruption age interpretation. *Geochemical Perspectives Letters*, *8*, 31–35. https://doi.org/10.7185/geochemlet.1826

Kelly, A. E., & Goulden, M. L. (2016). A montane Mediterranean climate supports year-round photosynthesis and high forest biomass. *Tree Physiology*, *36*(4), 459–468. https://doi.org/10.1093/treephys/tpv131

Konrad, W., Roth-Nebelsick, A., & Traiser, C. (2023). High productivity at high latitudes? Photosynthesis and leaf ecophysiology in Arctic forest of the Eocene. *Paleoceanography and Paleoclimatology*, *38*(8), e2023PA004685. https://doi.org/10.1029/2023PA004685

Körner, C., Möhl, P., & Hiltbrunner, E. (2023). Four ways to define the growing season. *Ecology Letters*, *26*(8), 1277–1292. https://doi.org/10.1111/ele.14260

Kowalski, E. A., & Dilcher, D. L. (2003). Warmer paleotemperatures for terrestrial ecosystems. *Proceedings of the National Academy of Sciences of the United States of America*, *100*(1), 167–170. https://doi.org/10.1073/pnas.232693599

Lionello, P., Malanotte-Rizzoli, P., Boscolo, R., Alpert, P., Artale, V., Li, L., et al. (2006). The Mediterranean climate: An overview of the main characteristics and issues. In *Developments in earth and environmental sciences* (Vol. 4, pp. 1–26). https://doi.org/10.1016/S1571-9197(06)80003-0

Lowe, A. J., Greenwood, D. R., West, C. K., Galloway, J. M., Sudermann, M., & Reichgelt, T. (2018). Plant community ecology and climate on an upland volcanic landscape during the Early Eocene Climatic Optimum: McAbee Fossil Beds, British Columbia, Canada. *Palaeogeography, Palaeoclimatology, Palaeoecology*, *511*, 433–448. https://doi.org/10.1016/j.palaeo.2018.09.010

Lunt, D. J., Bragg, F., Chan, W.-L., Hutchinson, D. K., Ladant, J.-B., Morozova, P., et al. (2021). DeepMIP: Model intercomparison of early Eocene climatic optimum (EECO) large-scale climate features and comparison with proxy data. *Climate of the Past*, *17*(1), 203–227. https://doi.org/10.5194/cp-17-203-2021

Mahon, K. I. (1996). The New "York" Regression: Application of an improved statistical method to geochemistry. *International Geology Review*, *38*(4), 293–303. https://doi.org/10.1080/00206819709465336

Mair, J. L., Hart, C. J., & Stephens, J. R. (2006). Deformation history of the northwestern Selwyn Basin, Yukon, Canada: Implications for orogen evolution and mid-Cretaceous magmatism. *Geological Society of America, Bulletin*, *118*(3–4), 304–323. https://doi.org/10.1130/B25763.1

Martinez, C., Jaramillo, C., Martínez-Murcia, J., Crepet, W., Cardenas, A., Escobar, J., et al. (2021). Paleoclimatic and paleoecological reconstruction of a middle to late Eocene South American tropical dry forest. *Global and Planetary Change*, *205*, 103617. https://doi.org/10.1016/j.gloplacha.2021.103617

Mavi, H. S., & Tupper, G. J. (2004). *Agrometeorology: Principles and applications of climate studies in agriculture*. CRC Press.

McCree, K. J. (1972). Test of current definitions of photosynthetically active radiation against leaf photosynthesis data. *Agricultural Meteorology*, *10*, 443–453. https://doi.org/10.1016/0002-1571(72)90045-3

McDermott, R. G., Ault, A. K., Caine, J. S., & Thomson, S. N. (2019). Thermotectonic history of the Kluane Ranges and evolution of the eastern Denali fault zone in southwestern Yukon, Canada. *Tectonics*, *38*(8), 2983–3010. https://doi.org/10.1029/2019TC005545

Methner, K., Mulch, A., Fiebig, J., Wacker, U., Gerdes, A., Graham, S. A., & Chamberlain, C. P. (2016). Rapid middle Eocene temperature change in western North America. *Earth and Planetary Science Letters*, *450*, 132–139. https://doi.org/10.1016/j.epsl.2016.05.053

Meyer, H. W. (2007). A review of paleotemperature–lapse rate methods for estimating paleoelevation from fossil floras. *Reviews in Mineralogy and Geochemistry*, *66*(1), 155–171. https://doi.org/10.2138/rmg.2007.66.6

Minnich, R. A. (2006). California climate and fire weather. In *Fire in California's ecosystems* (pp. 13–37). University of California Press.

Mulch, A., Chamberlain, C. P., Cosca, M. A., Teyssier, C., Methner, K., Hren, M. T., & Graham, S. A. (2015). Rapid change in high-elevation precipitation patterns of western North America during the Middle Eocene Climatic Optimum (MECO). *American Journal of Science*, *315*(4), 317–336. https://doi.org/10.2475/04.2015.02

Myking, T., & Heide, O. M. (1995). Dormancy release and chilling requirement of buds of latitudinal ecotypes of Betula pendula and B. pubescens. *Tree Physiology*, *15*(11), 697–704. https://doi.org/10.1093/treephys/15.11.697

New, M., Lister, D., Hulme, M., & Makin, I. (2002). A high-resolution data set of surface climate over global land areas. *Climate Research*, *21*(1), 1–25. https://doi.org/10.3354/cr021001

Nienstaedt, H. (1967). Chilling requirements in seven Picea species. *Silvae Genetica*, *16*, 65–68.

Paulsen, J., & Körner, C. (2014). A climate-based model to predict potential treeline position around the globe. *Alpine Botany*, *124*, 1–12. https://doi.org/10.1007/s00035-014-0124-0

Pavlis, T. L. (1989). Middle Cretaceous orogenesis in the northern Cordillera: A Mediterranean analog of collision-related extensional tectonics. *Geology*, *17*(10), 947–950. https://doi.org/10.1130/0091-7613(1989)017<0947:MCOITN>2.3.CO;2

Peel, M. C., Finlayson, B. L., & McMahon, T. A. (2007). Updated world map of the Köppen-Geiger climate classification. *Hydrology and Earth System Sciences*, *11*(5), 1633–1644. https://doi.org/10.5194/hess-11-1633-2007

Peppe, D. J., Baumgartner, A., Flynn, A., & Blonder, B. (2018). Reconstructing paleoclimate and paleoecology using fossil leaves. In D. A. Croft, D. F. Su, & S. W. Simpson (Eds.), *Methods in paleoecology* (pp. 289–317). Springer. https://doi.org/10.1007/978-3-319-94265-0_13

Peppe, D. J., Royer, D. L., Cariglino, B., Oliver, S. Y., Newman, S., Leight, E., et al. (2011). Sensitivity of leaf size and shape to climate: Global patterns and paleoclimatic applications. *New Phytologist*, *190*(3), 724–739. https://doi.org/10.1111/j.1469-8137.2010.03615.x

Poblete, F., Dupont-Nivet, G., Licht, A., Van Hinsbergen, D. J., Roperch, P., Mihalynuk, M. G., et al. (2021). Towards interactive global paleogeographic maps, new reconstructions at 60, 40 and 20 Ma. *Earth-Science Reviews*, *214*, 103508. https://doi.org/10.1016/j.earscirev.2021.103508

Poorter, H., Niinemets, Ü., Ntagkas, N., Siebenkäs, A., Mäenpää, M., Matsubara, S., & Pons, T. (2019). A meta-analysis of plant responses to light intensity for 70 traits ranging from molecules to whole plant performance. *New Phytologist*, *223*(3), 1073–1105. https://doi.org/10.1111/nph.15754

Pound, M. J., & Salzmann, U. (2017). Heterogeneity in global vegetation and terrestrial climate change during the late Eocene to early Oligocene transition. *Scientific Reports*, *7*(1), 1–12. https://doi.org/10.1038/srep43386

Reichgelt, T., Greenwood, D. R., Steinig, S., Conran, J. G., Hutchinson, D. K., Lunt, D. J., et al. (2022). Plant proxy evidence for high rainfall and productivity in the Eocene of Australia. *Paleoceanography and Paleoclimatology*, *37*(6), e2022PA004418. https://doi.org/10.1029/2022PA004418

Ridgway, K. D., Sweet, A. R., & Cameron, A. R. (1995). Climatically induced floristic changes across the Eocene-Oligocene transition in the northern high latitudes, Yukon Territory, Canada. *Geological Society of America, Bulletin*, *107*(6), 676–696. https://doi.org/10.1130/0016-7606(1995)107<0676:CIFCAT>2.3.CO;2

Rivero-Cuesta, L., Westerhold, T., Agnini, C., Dallanave, E., Wilkens, R. H., & Alegret, L. (2019). Paleoenvironmental changes at ODP site 702 (South Atlantic): Anatomy of the middle Eocene climatic optimum. *Paleoceanography and Paleoclimatology*, *34*(12), 2047–2066. https://doi.org/10.1029/2019PA003806

Rundel, P. W., Arroyo, M. T., Cowling, R. M., Keeley, J. E., Lamont, B. B., & Vargas, P. (2016). Mediterranean biomes: Evolution of their vegetation, floras, and climate. *Annual Review of Ecology, Evolution, and Systematics*, *47*(1), 383–407. https://doi.org/10.1146/annurev-ecolsys-121415-032330

Sarvas, R. (1972). Investigations on the annual cycle of development of forest trees. Active period. *Communicationes Instituti Forestalis Fenniae*, *76*, 1–110.

Schmidt, G. A., Kelley, M., Nazarenko, L., Ruedy, R., Russell, G. L., Aleinov, I., et al. (2014). Configuration and assessment of the GISS ModelE2 contributions to the CMIP5 archive. *Journal of Advances in Modeling Earth Systems*, *6*(1), 141–184. https://doi.org/10.1002/2013ms000265

Schneider, C. A., Rasband, W. S., & Eliceiri, K. W. (2012). NIH image to ImageJ: 25 years of image analysis. *Nature Methods*, *9*(7), 671–675. https://doi.org/10.1038/nmeth.2089

Scudder, G. G. E. (1997). Environment of the Yukon. In *Insects of the Yukon. Biological survey of Canada (terrestrial arthropods)* (pp. 13–57).

Sharman, G. R., Sharman, J. P., & Sylvester, Z. (2018). detritalPy: A Python-based toolset for visualizing and analysing detrital geothermochronologic data. *The Depositional Record*, *4*(2), 202–215. https://doi.org/10.1002/dep2.45

Shields, C. A., Kiehl, J. T., Rush, W., Rothstein, M., & Snyder, M. A. (2021). Atmospheric rivers in high-resolution simulations of the Paleocene Eocene Thermal Maximum (PETM). *Palaeogeography, Palaeoclimatology, Palaeoecology*, *567*, 110293. https://doi.org/10.1016/j.palaeo.2021.110293

Skwara, T., & Kurtz, L. (1988). Searching for fossils in Yukon and northwest territories. *Musk-Ox*, *36*, 29–37.

Sláma, J., Košler, J., Condon, D. J., Crowley, J. L., Gerdes, A., Hanchar, J. M., et al. (2008). Plešovice zircon—A new natural reference material for U–Pb and Hf isotopic microanalysis. *Chemical Geology*, *249*(1–2), 1–35. https://doi.org/10.1016/j.chemgeo.2007.11.005

Sluijs, A., Zeebe, R. E., Bijl, P. K., & Bohaty, S. M. (2013). A middle Eocene carbon cycle conundrum. *Nature Geoscience*, *6*(6), 429–434. https://doi.org/10.1038/ngeo1807

Spicer, R. A. (2008). CLAMP. In V. Gornitz (Ed.), *Encyclopedia of Paleoclimatology and ancient environments* (pp. 156–158). Springer. https://doi.org/10.1007/978-1-4020-4411-3

Spicer, R. A., Valdes, P. J., Spicer, T. E. V., Craggs, H. J., Srivastava, G., Mehrotra, R. C., & Yang, J. (2009). New developments in CLAMP: Calibration using global gridded meteorological data. *Palaeogeography, Palaeoclimatology, Palaeoecology*, *283*(1–2), 91–98. https://doi.org/10.1016/j.palaeo.2009.09.009

Spicer, R. A., Yang, J., Spicer, T. E., & Farnsworth, A. (2021). Woody dicot leaf traits as a palaeoclimate proxy: 100 years of development and application. *Palaeogeography, Palaeoclimatology, Palaeoecology*, *562*, 110138. https://doi.org/10.1016/j.palaeo.2020.110138

Stacey, J. S., & Kramers, J. D. (1975). Approximation of terrestrial lead isotope evolution by a two-stage model. *Earth and Planetary Science Letters*, *26*(2), 207–221. https://doi.org/10.1016/0012-821X(75)90088-6

Stefanidis, K., Varlas, G., Papaioannou, G., Papadopoulos, A., & Dimitriou, E. (2022). Trends of lake temperature, mixing depth and ice cover thickness of European lakes during the last four decades. *Science of the Total Environment*, *830*, 154709. https://doi.org/10.1016/j.scitotenv.2022.154709

Strong, T. R., & Driscoll, R. L. (2016). A process for reducing rocks and concentrating heavy minerals. *U.S. Geological Survey Open-File Report 2016–1022*, 16. https://doi.org/10.3133/ofr20161022

Sullivan, C., Stidham, T. A., Buryak, S., West, C. K., O'Connor, J. K., Reyes, A. V., et al. (2022). *A probable phaethontiform bird from the terrestrial Middle Eocene (Bartonian) of Yukon, Canada*. Society of Vertebrate Paleontology Annual Meeting 2022.

Tanino, K. K., Cherry, K. M., Kriger, J. N., Hrycan, W., Marufu, G., Thomas, J. D., & Gray, G. R. (2014). Photosynthetic responses to temperature-mediated dormancy induction in contrasting ecotypes of red-osier dogwood (*Cornus sericea* L.). *Environmental and Experimental Botany*, *106*, 221–230. https://doi.org/10.1016/j.envexpbot.2014.02.015

Taulavuori, K., Sarala, M., & Taulavuori, E. (2009). Growth responses of trees to Arctic light environment. In *Progress in botany* (Vol. 71, pp. 157–168). https://doi.org/10.1007/978-3-642-02167-1_6

Taylor, B. (1997). The climates of British Columbia and Yukon. *Responding to global climate change in British Columbia and Yukon*, *1*, 363.

Thimijan, R. W., & Heins, R. D. (1983). Photometric, radiometric, and quantum light units of measure: A review of procedures for interconversion. *HortScience*, *18*(6), 818–822. https://doi.org/10.21273/HORTSCI.18.6.818

Tierney, J. E., Zhu, J., Li, M., Ridgwell, A., Hakim, G. J., Poulsen, C. J., et al. (2022). Spatial patterns of climate change across the Paleocene–Eocene Thermal Maximum. *Proceedings of the National Academy of Sciences of the United States of America*, *119*(42), e2205326119. https://doi.org/10.1073/pnas.2205326119

Trop, J. M., Benowitz, J., Cole, R. B., & O'Sullivan, P. (2019). Cretaceous to Miocene magmatism, sedimentation, and exhumation within the Alaska Range suture zone: A polyphase reactivated terrane boundary. *Geosphere*, *15*(4), 1066–1101. https://doi.org/10.1130/GES02014.1

Trop, J. M., & Ridgway, K. D. (2007). Mesozoic and Cenozoic tectonic growth of southern Alaska: A sedimentary basin perspective. In K. D. Ridgway, J. M. Trop, J. M. G. Glen, & J. M. O'Neill (Eds.), *Tectonic growth of a collisional continental margin: Crustal evolution of southern Alaska* (Vol. 431, pp. 55–94). Geological Society of America Special Paper. https://doi.org/10.1130/2007.2431(04)

Trop, J. M., Ridgway, K. D., Manuszak, J. D., & Layer, P. (2002). Mesozoic sedimentary-basin development on the allochthonous Wrangellia composite terrane, Wrangell Mountains basin, Alaska: A long-term record of terrane migration and arc construction. *Geological Society of America, Bulletin*, *114*(6), 693–717. https://doi.org/10.1130/0016-7606(2002)114<0693:MSBDOT>2.0.CO;2

Valiente-Banuet, A., Flores-Hernàndez, N., Verdú, M., & Dàvila, P. (1998). The chaparral vegetation in Mexico under nonmediterranean climate: The convergence and Madrean-Tethyan hypotheses reconsidered. *American Journal of Botany*, *85*(10), 1398–1408. https://doi.org/10.2307/2446398

van Hinsbergen, D. J., De Groot, L. V., van Schaik, S. J., Spakman, W., Bijl, P. K., Sluijs, A., et al. (2015). A paleolatitude calculator for paleoclimate studies. *PLoS One*, *10*(6), e0126946. https://doi.org/10.1371/journal.pone.0126946

Vavrek, M. J., Evans, D. C., Braman, D. R., Campione, N. E., & Zazula, G. D. (2012). A Paleogene flora from the upper Bonnet Plume Formation of northeast Yukon Territory, Canada. *Canadian Journal of Earth Sciences*, *49*(3), 547–558. https://doi.org/10.1139/e11-073

Vermeesch, P. (2018). IsoplotR: A free and open toolbox for geochronology. *Geoscience Frontiers*, *9*(5), 1479–1493. https://doi.org/10.1016/j.gsf.2018.04.001

Vermeesch, P. (2021). Maximum depositional age estimation revisited. *Geoscience Frontiers*, *12*(2), 843–850. https://doi.org/10.1016/j.gsf.2020.08.008

Wareing, P. F. (1956). Photoperiodism in woody plants. *Annual Review of Plant Physiology*, *7*(1), 191–214. https://doi.org/10.1146/annurev.pp.07.060156.001203

Welander, N. T., & Ottosson, B. (1997). Influence of photosynthetic photon flux density on growth and transpiration in seedlings of Fagus sylvatica. *Tree Physiology*, *17*(2), 133–140. https://doi.org/10.1093/treephys/17.2.133

West, C. K., Greenwood, D. R., & Basinger, J. F. (2015). Was the Arctic Eocene 'rainforest' monsoonal? Estimates of seasonal precipitation from early Eocene megafloras from Ellesmere Island, Nunavut. *Earth and Planetary Science Letters*, *427*, 18–30. https://doi.org/10.1016/j.epsl.2015.06.036

West, C. K., Greenwood, D. R., & Basinger, J. F. (2019). The late Paleocene to early Eocene Arctic megaflora of Ellesmere and Axel Heiberg islands, Nunavut, Canada. *Palaeontographica Abteilung B*, *300*(1–6), 47–163. https://doi.org/10.1127/palb/2019/0066

West, C. K., Greenwood, D. R., Reichgelt, T., Lowe, A. J., Vachon, J. M., & Basinger, J. F. (2020). Paleobotanical proxies for early Eocene climates and ecosystems in northern North America from middle to high latitudes. *Climate of the Past*, *16*(4), 1387–1410. https://doi.org/10.5194/cp-16-1387-2020

West, C. K., Reichgelt, T., & Basinger, J. F. (2021). The Ravenscrag Butte flora: Paleoclimate and paleoecology of an early Paleocene (Danian) warm-temperate deciduous forest near the vanishing inland Cannonball Seaway. *Palaeogeography, Palaeoclimatology, Palaeoecology*, *576*, 110488. https://doi.org/10.1016/j.palaeo.2021.110488

West, C. K., Reichgelt, T., Reyes, A. V., Buryak, S. D., Staniszewska, K. J., & Basinger, J. F. (2024). Paleobotanical evidence for Mediterranean climates in the western Canadian paleoarctic during the late middle Eocene [Dataset]. *figshare*. https://doi.org/10.6084/m9.figshare.25213451

Westerhold, T., Marwan, N., Drury, A. J., Liebrand, D., Agnini, C., Anagnostou, E., et al. (2020). An astronomically dated record of Earth's climate and its predictability over the last 66 million years. *Science*, *369*(6509), 1383–1387. https://doi.org/10.1126/science.aba6853

Wiedenbeck, M. A. P. C., Alle, P., Corfu, F. Y., Griffin, W. L., Meier, M., Oberli, F. V., et al. (1995). Three natural zircon standards for U-Th-Pb, Lu-Hf, trace element and REE analyses. *Geostandards Newsletter*, *19*(1), 1–23. https://doi.org/10.1111/j.1751-908X.1995.tb00147.x

Wilf, P. (1997). When are leaves good thermometers? A new case for leaf margin analysis. *Paleobiology*, *23*(3), 373–390. https://doi.org/10.1017/S0094837300019746

Wilf, P., Wing, S. L., Greenwood, D. R., & Greenwood, C. L. (1998). Using fossil leaves as paleo precipitation indicators: An Eocene example. *Geology*, *26*(3), 203–206. https://doi.org/10.1130/0091-7613(1998)026<0203:UFLAPI>2.3.CO;2

Willard, D. A., Donders, T. H., Reichgelt, T., Greenwood, D. R., Sangiorgi, F., Peterse, F., et al. (2019). Arctic vegetation, temperature, and hydrology during Early Eocene transient global warming events. *Global and Planetary Change*, *178*, 139–152. https://doi.org/10.1016/j.gloplacha.2019.04.012

Williams, C. J., LePage, B. A., Johnson, A. H., & Vann, D. R. (2009). Structure, biomass, and productivity of a late Paleocene Arctic forest. *Proceedings of the Academy of Natural Sciences of Philadelphia*, *158*(1), 107–127. https://doi.org/10.1635/053.158.0106

Williams, I. S. (1998). U–Th–Pb geochronology by ion microprobe. *Reviews in Economic Geology*, *7*, 1–35. https://doi.org/10.5382/Rev.07.01

Wing, S. L., & Greenwood, D. R. (1993). Fossils and fossil climate: The case for equable continental interiors in the Eocene. *Philosophical Transactions of the Royal Society of London. Series B: Biological Sciences*, *341*(1297), 243–252. https://doi.org/10.1098/rstb.1993.0109

Wolfe, J. A. (1993). *A method of obtaining climatic parameters from leaf assemblages* (Vol. 2040). U.S. Geological Survey, Bulletin. https://doi.org/10.3133/b2040

Yalcin, F., & Arca, D. (2024). Investigation and comparison of climate boundary maps generated with various climate. In *Interdisciplinary studies on contemporary research practices in Engineering in the 21st Century-VI* (p. 33). https://doi.org/10.58830/ozgur.pub426.c1847

Yang, J., Spicer, R. A., Spicer, T. E., Arens, N. C., Jacques, F. M., Su, T., et al. (2015). Leaf form–climate relationships on the global stage: An ensemble of characters. *Global Ecology and Biogeography*, *24*(10), 1113–1125. https://doi.org/10.1111/geb.12334

Yang, J., Spicer, R. A., Spicer, T. E. V., & Li, C.-S. (2011). CLAMP' Online: A new web-based palaeoclimate tool and its application to the terrestrial Paleogene and Neogene of North America. *Palaeobiodiversity and Palaeoenvironments*, *91*(3), 163–183. https://doi.org/10.1007/s12549-011-0056-2

Young, F. G. (1975). *Upper Cretaceous stratigraphy, Yukon coastal plain and northwestern Mackenzie delta* (Vol. 249, pp. 1–83). Geological Survey of Canada, Bulletin. https://doi.org/10.4095/103975

Zachos, J. C., Dickens, G. R., & Zeebe, R. E. (2008). An early Cenozoic perspective on greenhouse warming and carbon-cycle dynamics. *Nature*, *451*(7176), 279–283. https://doi.org/10.1038/nature06588

Zhang, X., Li, J., Wang, Z., & Dong, Q. (2022). Global hydroclimatic drivers of terrestrial water storage changes in different climates. *Catena*, *219*, 106598. https://doi.org/10.1016/j.catena.2022.106598

Zhu, J., Poulsen, C. J., & Otto-Bliesner, B. L. (2020). High climate sensitivity in CMIP6 model not supported by paleoclimate. *Nature Climate Change*, *10*(5), 378–379. https://doi.org/10.1038/s41558-020-0764-6